

Universidad Autónoma de San Luis Potosí

Instituto de Física

Flexible composite phase change films enhanced by hectorite and graphene nanoplates

Tesis para obtener el grado de

Maestro en Ciencias Interdisciplinarias

Presentado por

Keqiao Gao

co-dirigida por

Dr. Shaoxian Song

Dr. Bernardo José Luis Arauz Lara

San Luis Potosí, S.L.P , México. 2024

Abstract

Phase change materials (PCMs) are essential for improving energy efficiency in thermal management systems, yet their widespread adoption is hindered by challenges such as flammability and low thermal conductivity. This thesis explores the integration of hectorite and graphene nanoplatelets (GNP) into flexible PCMs to address these limitations and expand their use in various applications. The incorporation of hectorite significantly bolsters the mechanical and fire retardant properties of PCMs. Experiments reveal that flexible PCMs with 15% hectorite content demonstrate an increase in tensile strength to 16.84 MPa and a reduction in fracture strain to 3.27%, which is a marked improvement over PCMs without hectorite, which exhibit a tensile strength of 9.56 MPa and a fracture strain of 3.92%. Furthermore, the addition of GNP has profoundly enhanced the thermal conductivity and phase change efficiency of polyethylene glycol/cellulose nanofiber (PEG/CNF) composite films. The introduction of 5% GNP elevates the thermal conductivity coefficient to 3.22 W/mK, and with 15% GNP, it further escalates to 12.2 W/mK, a substantial rise from the base composite's conductivity of 0.184 W/mK. This enhancement is critical for applications requiring swift and efficient heat management. Practical tests of these enhanced PCMs in building management, wearable technology, and electronics illustrate their versatility. In building applications, these materials stabilize indoor temperatures, effectively reducing energy demands for heating and cooling systems. For wearable technologies, the PCMs help maintain stable skin temperatures, enhancing user comfort and safety. In electronics, these materials adeptly manage heat, preventing overheating and extending device longevity. This research highlights the successful integration of hectorite and GNP in overcoming the traditional limitations of PCMs, significantly enhancing their functionality and safety. The findings bridge the gap between laboratory research and practical implementation, suggesting that the advanced PCM composites have the potential to revolutionize thermal management practices across diverse sectors.

Table of Contents

List of Figures

List of Tables

1. Introduction

1.1 Background

With the comprehensive advancement of human industrialization and intelligentization, global energy consumption has surged annually, marking significant impacts on economic growth, environmental stability, and societal well-being[1], [2], [3], [4]. The prevailing model of energy consumption, primarily reliant on fossil fuels, exacerbates significant societal challenges such as energy shortages, an unbalanced energy mix, environmental pollution, and climate change[5], [6]. This traditional dependency on fossil energy sources has led to heightened global concerns about the sustainability of such practices and their long-term ecological impacts. Confronted with the daunting energy crisis, scientific researchers worldwide are dedicated to identifying new energy sources that can replace fossil fuels. In this pursuit, the focus has expanded to include not only the replacement of these traditional sources but also the enhancement of energy efficiency and the reduction of carbon footprints. Currently, the emphasis is on exploring renewable energies like solar, wind, hydro, and nuclear energy as viable alternatives to conventional fossil fuels. These sources, due to their abundant availability, renewability, and minimal environmental impact, are increasingly regarded as essential to global energy strategies aimed at achieving sustainable development goals. Renewable energy's role extends beyond simple energy provision to encompass critical aspects of modern energy systems, including grid stability, energy security, and access to clean and affordable energy [7], [8]. In recent years, the potential of thermal energy as a renewable resource has gained traction. With its capacity to balance supply and demand discrepancies and provide sustainable energy solutions, thermal energy is poised to become a significant component of the renewable energy matrix[9], [10], [11]. It offers unique opportunities for integration into existing energy systems and for facilitating the transition toward low-carbon economies.

1.1.1 Thermal energy storage

Thermal Energy Storage (TES) technology can be categorized into three distinct methods: sensible heat storage, latent heat storage, and chemical heat storage. The thermal performance of a TES system largely depends on the thermal properties of the storage medium used [12]. Sensible heat storage employs media that do not change phase during use, achieving heat storage or release through the heating or cooling of the medium. Water, the most commonly used medium in sensible heat storage, is the most mature technology in this category. However, it has a relatively low energy storage density because it depends solely on temperature changes of the medium to store energy[13], [14]. Thermochemical heat storage utilizes reversible thermochemical reactions to store and release heat. Although it offers high energy storage density, the reaction temperatures required are extremely high, ranging from 400 to 1000 degrees Celsius. These reactions often involve the generation and interaction of high-pressure gases, and the chemicals can be corrosive to containers. This makes chemical heat storage systems highly demanding in terms of material

quality and challenging to implement for everyday use[15], [16]. Latent heat storage, on the other hand, harnesses the latent heat from phase changes of the storage medium to efficiently store and reuse heat. This process keeps the temperature of the medium almost constant during the phase change. Among various phase transitions—such as liquid-gas, solid-gas, and solid-liquid—the most commonly utilized is the solid-liquid transition due to the minimal volume change between these states[17], [18], [19], [20]. In contrast, the large volume difference between gas and the other two states presents significant challenges in designing effective phase change material seals for gas transformations. Due to its practical value, the solid-liquid phase change material has increasingly become the focus of research and is seen as a promising area for future energy solutions.

1.1.2 Phase change materials

Phase change materials (PCMs) play a pivotal role in enhancing energy storage and efficiency through latent heat technology. These materials operate on the principle of absorbing or releasing large amounts of heat while maintaining a consistent temperature during the phase transition process[21], [22]. Specifically, in environments where the temperature is high, solid-liquid PCMs absorb excess heat and melt, effectively reducing the surrounding temperature. Conversely, in cooler conditions, these materials release stored heat and solidify, thereby raising the ambient temperature.

PCMs are broadly categorized into three types: inorganic, organic, and eutectic[23]. Inorganic PCMs, which include metals and salt hydrates, are characterized by their significant supercooling effects and high corrosiveness, which can lead to uneven melting and chemical instability[24], [25], [26]. Organic PCMs, such as paraffin, fatty acids, esters, and alcohols, though faced with challenges like low thermal conductivity and flammability, are noted for their stable chemical and thermal properties. They exhibit minimal supercooling, are non-corrosive, and melt uniformly, making them cost-effective for wide-scale use [27], [28], [29]. Eutectic PCMs represent a hybrid category, consisting of mixtures of two or more substances that have similar melting points and are compatible. These can be combinations of either inorganic-inorganic, inorganic-organic, or organic-organic materials. Despite their tailored melting points and compatibility, eutectic PCMs often involve higher research and development costs and are characterized by lower latent heat capacity and higher overall costs, which can impede their broader application and development[30], [31], [32].Among these, organic PCMs stand out due to their practical viability. Their stable chemical and thermal behavior, coupled with cost-effectiveness, make them particularly attractive for applications requiring efficient and economical thermal energy management solutions. This suitability positions organic PCMs as a preferred choice for advancing TES technologies, especially in sectors striving for cost-effective and sustainable energy solutions.

1.1.3 Flexible phase change material

Solid-liquid organic PCMs are often challenged by the issue of liquid leakage, presenting a significant barrier to their practical application in thermal management systems[33], [34], [35].

Traditional macro-encapsulation techniques, while effective in containing the liquid PCM, often suffer from limited versatility and require custom encapsulation shapes to suit specific applications, restricting their broader use[36]. To address the leakage issue without the constraints of bulk encapsulation, alternative approaches have been developed. One such method involves impregnating the PCM within a porous support matrix, which allows for the containment of the PCM while maintaining the material's integrity[37], [38], [39]. Further advancements in the containment of PCMs include microencapsulation and polymer grafting techniques. Microencapsulation involves encasing micro-particles of the PCM within durable shell materials, effectively preventing leakage while allowing thermal exchange[40], [41], [42], [43]. Polymer grafting takes a different approach by chemically bonding the PCM to polymer chains, forming a cross-linked molecular structure that integrates the thermal storage properties of PCMs with the mechanical stability of polymers[44], [45], [46]. These innovative encapsulation solutions—impregnation into porous matrix, microencapsulation, and polymer grafting—not only overcome the challenges of liquid leakage but also enhance the functional integration of PCMs into various applications.

The three encapsulation methods described above enable the creation of flexible PCMs, which offer distinct advantages over traditional rigid and brittle PCMs. Flexible PCMs effectively address the issues of damage susceptibility by offering enhanced durability and resilience[47], [48], [49], [50]. Moreover, these materials optimize the contact area with the target object, significantly reducing the air gaps that typically exist between contact surfaces[51], [52], [53], [54]. Since air conducts heat poorly, minimizing these gaps effectively increases the effective thermal contact area, thereby enhancing heat transfer. Furthermore, flexible PCMs offer logistical advantages during storage and transport, as they can be compacted into smaller volumes compared to customized, rigid alternatives. Their flexibility also simplifies installation and removal processes, making them highly practical for various applications[55]. To date, the use of flexible PCMs in areas such as thermal management for electronic components, personal thermal regulation, flexible sensors, and sustainable building thermal management has demonstrated considerable potential, highlighting their transformative capabilities in these fields.

1.1.4 Drawbacks of organic flexible PCM

This section will delve deeper into the challenges associated with organic flexible PCMs. Organic PCMs, despite their advantages, exhibit critical drawbacks such as flammability and low thermal conductivity. These limitations pose significant hurdles to their broader application. For instance, the use of flammable materials in green building construction introduces potential fire hazards, necessitating measures to mitigate the flammability of organic PCMs[56], [57]. Additionally, the low thermal conductivity of organic PCMs can restrict their use in thermal management systems that require swift thermal responses[58], [59], [60]. This low conductivity results in inadequate heat transfer between the PCMs and the objects they are intended to regulate, thereby diminishing the efficiency of heat utilization. Such constraints narrow the scope of applications for organic PCMs, which are currently favored in areas like thermal insulation and

infrared shielding. Addressing the issue of low thermal conductivity could significantly expand the potential applications of organic PCMs, enhancing their effectiveness in a broader array of thermal management scenarios. Overcoming these challenges is essential for maximizing the utility and adoption of organic PCMs in diverse industries.

Despite recent advancements in the development of flexible PCMs, the field remains ripe for further exploration and innovation. Research into flexible PCMs is still in its early stages, particularly in balancing the inherent trade-off between flexibility and mechanical strength[55], [61]. This dilemma stems from the limitations of current encapsulation or support materials, which typically struggle to provide high flexibility and substantial mechanical strength simultaneously. As flexible PCMs are a relatively novel area of study, there is a noticeable gap in research efforts aimed at enhancing their mechanical properties without compromising their flexibility. Strengthening the mechanical durability of flexible PCMs is crucial because materials that can withstand repeated bending and folding without degradation are more suited to dynamic applications and have a significantly extended service life. Enhancing the durability and resilience of these materials not only expands their practical applications but also boosts their economic viability[62], [63]. For instance, more durable flexible PCMs can be integrated into wearable technology, flexible electronics, and smart textiles, where they can provide effective thermal management without the risk of mechanical failure. Addressing these challenges and advancing the technology of flexible PCMs will open new avenues for their adoption across various sectors, ultimately leading to broader implementation and promotion of these innovative materials. Moreover, the incorporation of emerging functionalities into flexible phase change films can further broaden their range of applications. By enhancing properties such as the photothermal effect, electrical conductivity, or electrothermal conversion, these advanced materials can be tailored to meet specific industry needs. Enhancements in photothermal efficiency could enable more effective solar energy utilization, while improved electrical conductivity might allow for integration into smart electronic systems[64], [65], [66], [67]. Additionally, advances in electrothermal conversion capabilities could facilitate innovative applications in energy generation and storage sectors. Expanding these functional attributes not only diversifies the potential uses of flexible PCMs but also contributes to their technological advancement and commercial viability. Integrating such multifunctional capabilities positions these materials as crucial components in the development of adaptive, energy-efficient technologies.

1.2 Objective

Building on the foundational work in PCMs, this thesis aims to significantly enhance the capabilities and applications of flexible PCMs through several focused objectives. The first objective of this study is to develop enhanced flexible PCMs by incorporating innovative substances such as hectorite and graphene nanoplatelets (GNP). By integrating these materials, this research seeks not only to improve the mechanical strength and durability of PCMs but also to optimize their thermal storage capabilities. The introduction of hectorite is expected to enhance fire resistance and structural integrity, while GNP will be explored for their potential to increase

thermal conductivity and mechanical properties. This approach is anticipated to overcome the traditional limitations of flexibility versus strength in PCMs, providing more robust and versatile solutions suitable for a wider range of applications. Furthermore, this research aims to extend the functionality of flexible PCMs by integrating advanced properties such as enhanced photothermal effects and improved electrothermal conversion capabilities. Exploring these functionalities will allow the materials to be used in innovative applications such as solar energy harvesting and smart thermal regulation systems. By enhancing the photothermal and electrothermal properties, this study seeks to create PCMs that not only manage heat effectively but also contribute to energy generation and savings, aligning with the needs of modern technological and sustainable development. Another major objective is to rigorously evaluate the thermal efficiency and mechanical robustness of the newly developed flexible PCMs under conditions that simulate real-world applications. The effectiveness of these materials will be tested in scenarios relevant to green building design and electronic devices, which require high levels of thermal management and energy efficiency. This testing will help determine the practicality of the PCMs in actual environmental conditions and establish their performance benchmarks. Through these objectives, the thesis will address critical gaps in the current technology of PCMs, pushing forward the boundaries of their applications and demonstrating their potential in new, demanding environments.

1.3 Research contents

According to the previous part, the challenges in the development of organic flexible PCMs. Despite their benefits, these materials face issues like flammability and low thermal conductivity, limiting their use in applications requiring rapid thermal responses and increasing fire risks in scenarios such as green building. The field, still in its infancy, struggles with balancing flexibility and mechanical strength, impeding broader application and innovation. Future research aims to enhance mechanical durability and integrate advanced functionalities like photothermal effects and electrothermal conversion to expand their utility in sectors like solar energy and smart electronics. Addressing these challenges could transform the practical deployment and efficiency of flexible PCMs across various industries. By addressing these challenges, the thesis aims to transform the efficiency and scope of flexible PCMs in various sectors. To systematically address these innovations, the thesis is organized into three focused chapters. Each chapter explores different facets of material enhancement with hectorite and GNP, promising to significantly improve the performance and versatility of PCMs.

1) Assesses the addition of hectorite to flexible PCMs, focusing on improving fire resistance, structural integrity, and mechanical strength. It provides a background on the unique properties of hectorite, discusses experimental results showcasing its beneficial impact on the thermal stability and fire resistance of PCMs, and concludes with implications for enhancing safety and durability in various PCM applications.
2) Explores the incorporation of GNP to boost the thermal conductivity and mechanical properties of flexible PCMs. It begins with an overview of graphene's remarkable properties, presents data analyzing its effect on enhancing thermal management

capabilities and the structural robustness of PCMs, and considers the broader application potential of GNP-enhanced PCMs in terms of energy efficiency and performance.

3) Demonstrates the real-world applications of enhanced flexible PCMs in green building, wearable technology, and electronic devices. It includes case studies that illustrate the practical effectiveness of these materials in managing thermal conditions, discusses the economic, environmental, and technological impacts of their deployment, and assesses their role in advancing sustainable technology solutions.

2. Materials and experiment

2.1 Materials and equipment

2.1.1 Materials

Please see the attached Table 1. for the regents used during the experiment.

Table 1. Lists of the reagents used during the experiment.

Reagent	Formula	Supply company
Calcium chloride	$CaCl_2$	Sigma Aldrich Chemicals Pvt. Ltd
Deionized water	H_2O	Generated by Milli-Q ultra-pure water meter
Graphene nanoplatelets	C	Kaina Carbon New Materials Co., Ltd.
Hectorite	$Na^{+0.7}$ $[Si_8Mg_{5.5}Li_{0.3}O_{20}(OH)_4)]^{-0.7}$	Hemings Technology Co., Ltd.
Polyethylene Glycol 4000	$HOCH_2(CH_2OCH_2)_nCH_2OH$	Shanghai Wulian Chemical Plant
Polyethylene Glycol 6000	$HOCH_2(CH_2OCH_2)_nCH_2OH$	Shanghai Wulian Chemical Plant
Polyethylene Glycol 800	$HOCH_2(CH_2OCH_2)_nCH_2OH$	Shanghai Wulian Chemical Plant
Tempo-oxidized Cellulose Nanofiber	-	Tianjin Wood Spirit Biotechnology Co., Ltd.

2.1.2 Equipment

Please refer the attached Table 2 for the equipment used during the study.

Table 2. Lists of equipment used throughout the study.

Equipment	Model	Supply company
Atomic Force Microscope	Multimode 8	Bruker Corporation (U.S.)
Differential Scanning Calorimeter	Q2000	TA Instruments (U.S.)
Electric Drying Oven with Forced Convection	WGL-125B	Tianjin Test Instrument Co., LTD (China)

Electronic Scales	ME 104	Mettler Toledo Instruments Shanghai Co., LTD (Switzerland)
Electronic Scales	YP6002	Shanghai Youke Instrument Co., LTD, China
Fourier Transform Infrared Spectrometer	iS20	Thermo Fisher Scientific™ Nicolet™ (U.S.)
High Shear Dispersion Emulsifier	FA25	FLUKO Shanghai Equipment Co., Ltd (Germany)
Micro Combustion Calorimeter	MCC-3	Deatak, Inc (U.S.)
Microcomputer Controlled Electro-Hydraulic Servo Universal Testing Machine	Instron 5969	Illinois Tool Works Inc. (U.S.)
Scanning Electron Microscope	SU8010	Hitachi, Ltd. (Japan)
Thermal Conductivity Meter	TPS 2500S	Hot Disk AB (Sweden)
Thermal Infrared Camera	FOTRIC 224S	Shanghai Jianling electronic Technology Co., LTD (U.S.)
Thermostatic Magnetic Stirrer	524G	Shanghai Meiyingpu instrument manufacturing company (China)
Thermogravimetry Analysis	449F3	NETZSCH Group (Germany)
Vacuum Freeze Dryer	LGJ-12	Beijing Songyuan Technology Development Co., LTD (China)
Water Purification Equipment	Direct 8	Merck Millipore Co., LTD (U.S.)
Xenon Lamp	PL-MW2000	Beijing Poferai Technology Co., LTD (China)
X-ray Diffraction Meter	D8	Bruker Corporation (U.S.)

2.2 Methodology

2.2.1 Synthesis

In this study, different composite flexible PCMs were prepared, and their preparation methods were described in the first section of chapter 3 an 4.

2.3 Characteristic

2.3.1 Scanning electron microscope（SEM）

The SEM is conducted to investigate the surface micro-characterization of the synthesized material throughout the study. The model SU8010 (Hitachi, Ltd. Japan) was employed in this study to determine the material surface micro topography and the elements distribution. The sample was freeze dried prior to the test, and then was gold sprayed due to the poor electrical conductivity of the samples. During the SEM test, the acceleration voltage was set at 5-10 kV under vacuum condition.

2.3.2 Atomic force microscope（AFM）

The AFM Multimode 8 (Bruker, U.S.) was utilized to study the particle size and the thickness of the nano particles. The sample preparation procedure involves initially suspending the sample in water, followed by using a homogenizer to ensure its uniform dispersion onto a mica

substrate, and then airdried under a dust-free environment. Measurement was carried out at room temperature, using a scan size of 5nm x 5nm at a scan rate of 1Hz, and the peak force setpoint is set at 0.15V.

2.3.3 Fourier transform infrared spectrometer（FTIR）

The FTIR analysis was conducted using an iS20 (Nicolet™, U.S.) to determine the functional group in the sample hence to study the synthetic mechanism of the flexible PCM film. The particle sample was grinded in an agate mortar, followed by pressing into 13mm palettes under vacuum, while the film sample was tested under the attenuated total reflectance (ATR) mode, the range for the wavelength is from 4000 - 400cm^{-1} and an accumulation of 32 scans is employed to enhance the resolution.

2.3.4 Differential scanning calorimeter（DSC）

The DSC measurement was performed using a Q2000 (TA instruments, U.S.). Approximately 5 mg of the sample was weighted and sealed in standard aluminum pans. The instrument was calibrated using high-purity indium and zinc standards prior to the measurements. And samples were analyzed user a nitrogen atmosphere with a flow rate of 50 mL/min to prevent oxidation for the sample. The temperature program various due to the different fusion temperatures of the samples, but the overall temperature was raised to the highest point and dropped to the lowest temperature with the constant temperature changing rate of 1°C/min, and no isothermal holds were employed in this study.

2.3.5 Thermal analyzer（TG）

The TGA analysis was carried out using a 449F3 (NETZSCH STA, Germany). Firstly, the sample weighted approximately 10 mg was placed in a aluminum crucible and subjected to a temperature ramp from 30°C to 500°C at a rate of 10 k/min under a nitrogen atmosphere with a flow rate of 50 mL/min. The temperature program consisted of a single continuous heating sequence without any isothermal holds.

2.3.6 Thermal conductivity meter（Hot Disk）

The thermal conductivity properties of the sample were measured using a TPS 2500S (Hot Disk AB, Sweden). The power samples were grinded in an agate mortar, followed by pressing into identical palette with diameter of 30 mm, and the film samples were tailored to identical discs with diameters of 30 mm, ensuring the sensor was fully encapsulated with no exposure. Prior to testing, the calibration was verified using a standard reference with known thermal conductivity. Measurements were carried out at room temperature (30°C), with a sensor power of 0.1 W and test duration of 10 s. Three repeated measurements were performed on each sample to ensure reproducibility, and the results were averaged with standard deviation calculated for each thermal property.

2.3.7 Micro calorimeter（MCC）

The micro calorimetric measurements were conducted using a micro combustion calorimeter MCC-3 (Deatak, U.S.). Approximately 5 mg of the sample was grounded and then placed in the steel calorimetric cell. Prior to testing, the instrument was calibrate using certified polyethylene standards. The combustion tests were carried out under a controlled atmosphere consisting of 20% oxygen balanced with nitrogen, at a flow rate of 100 mL/min. The temperature program involved heating the sample at a rate of 1°C/s up to 900°C. Data on heat release rate and mass loss were captured using the calorimeter's integrated data acquisition system and analyzed using MCC analysis software. Each sample was tested in triplicate to ensure reproducibility of the results.

2.3.8 Thermal infrared camera

The thermal imaging was performed using a thermal infrared camera 224s (FOTRIC, U.S.). The camera was calibrated using a blackbody source before each series of measurements, and the measurements were taken from a distance of approximately 50 cm. AnalyzIR was employed to analyze the collected graphs. The camera was mounted on a tripod to ensure stability and minimized measurement variations, and results were cross verified by repeating measurements under similar conditions.

2.3.9 Microcomputer controlled electro-hydraulic servo universal testing machine

The mechanical properties of the flexible film samples were evaluated using a microcomputer controlled electro-hydraulic servo universal testing machine Instron 5969 (Illinois tool works, U.S.). The samples were prepared as 30 mm x 1 mm film. Each sample was subjected to a tensile test at a constant displacement rate of 0.02 mm/min. Data from a minimum of 8 replicated per sample type were analyzed to calculate the mean mechanical properties.

3. Hectorite enforcing mechanical strength and flame retardancy of flexible phase change film

3.1 Synthesis Method

The flexible hectorite enforced phase change film were produced using the following procedures, with water as the medium. At first, various determined proportions of PEG and hectorite were added into the beaker with quantified volume of pure water. This mixture was then magnetically stirred at 500 rpm for 30 mins to achieve complete dissolution and homogenous distribution. After the dispersing process, a set amount of CNF was introduced into the mixture, and then it's subjected to high shear emulsification machine at 8000 rpm for 15 mins. This mixture

was then degassed under vacuum for another 15 mins before transferred into a polytetrafluoroethylene mold to facilitate crosslinking for 12 hrs. Next, the formed hydrogel was then soaked in a 1 wt.% calcium chloride solution for 10 mins to allow further crosslinking and subsequently rinsed thoroughly with deionized water. The gel was then left to airdry at ambient temperature for 48 hrs. A schematic of the synthetic process is shown in Fig. 1, and varying percentages of components are detailed in Table. 3.

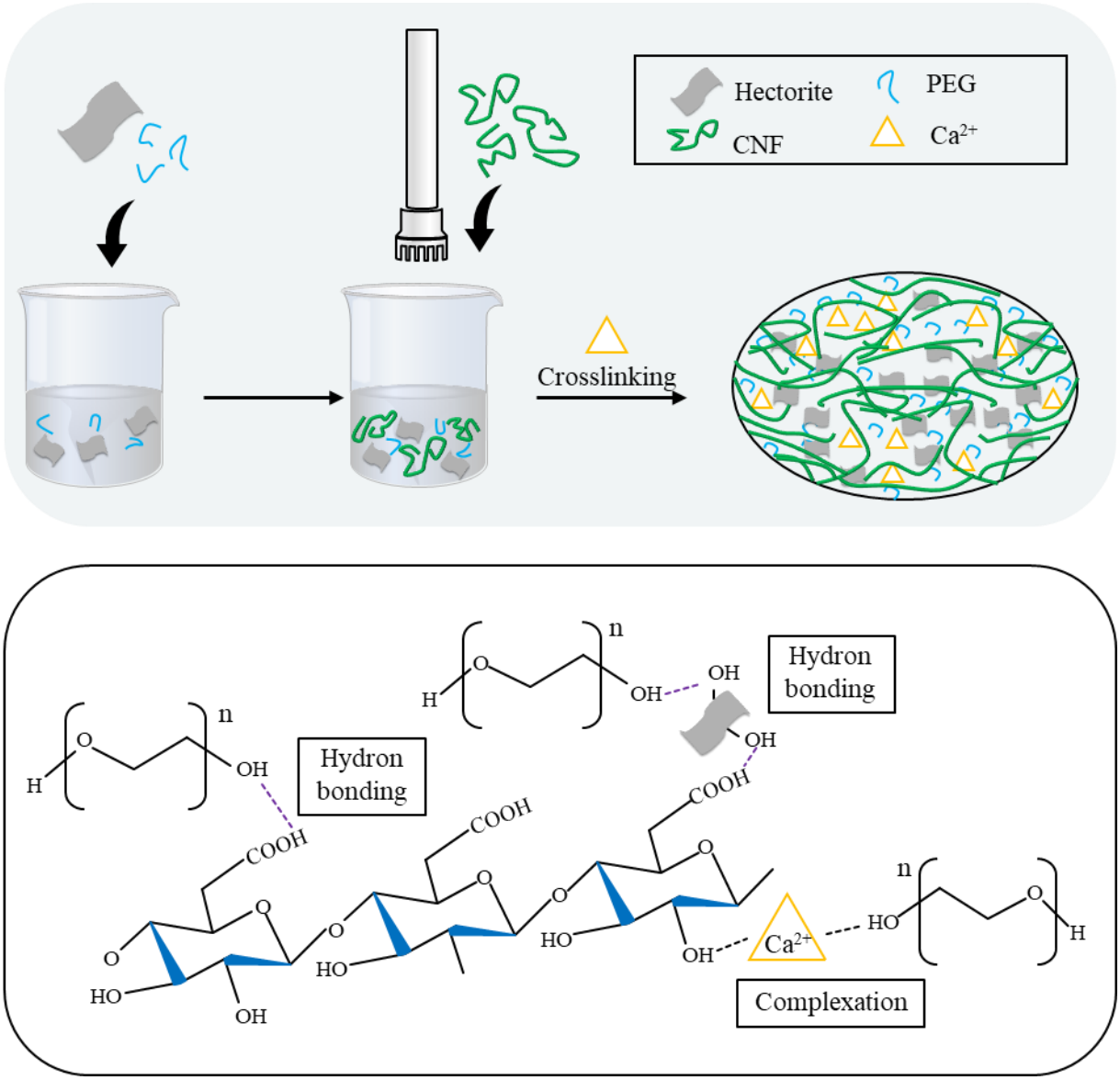

Figure 1. Schematic diagram for synthesizing PEG/hectorites/CNF composite flexible PCM.

Table 3. Sample composition ratios for hectorite enforcing PCM film.

Sample name	PEG (wt.%)	CNF (wt.%)	Hectorite (wt.%)
PEG/CNF	70	30	0

PEG/CNF/Hectorite5%	70	25	5
PEG/CNF/Hectorite10%	70	20	10
PEG/CNF/Hectorite15%	70	15	15

3.2 Characteristics and synthesis mechanism

3.2.1 Characteristics

This section introduces the macroscopic observations and microscopic features of the film. For macroscopic aspect, digital photos of the prepared composite PCM samples are presented in Fig. 2, capturing various states of deformation. These include bending as shown in Fig. 2a, tailored and folded configurations in Fig. 2b, and a state with no deformation in Fig. 2c. These images illustrate the composite film's outstanding flexibility and shape stability. Furthermore, the films that is not deformed was created using a large-sized mold measuring 15 cm by 25 cm, demonstrating its suitability for large-scale production. This indicates the material's potential for widespread manufacturing applications, where maintaining form and integrity under varying physical conditions is critical.

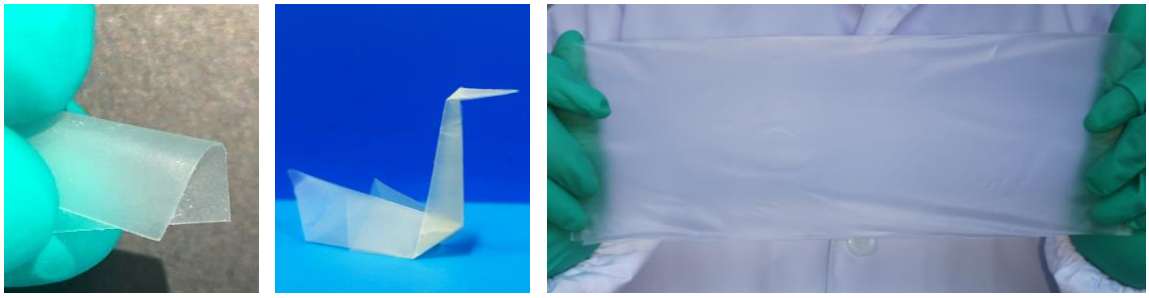

Figure 2. Digital photo of the composite PEG/CNF/Hectorite15% film samples (a) bended, (b) tailored and folded, (c) under no deformation.

As for microscopic aspect, the morphological structure of CNF films was analyzed using Scanning Electron Microscopy (SEM), as depicted in Fig. 3, which highlights the cross-sectional SEM images of PEG/CNF/Hectorite15% films. The microarchitecture of these flexible films reveals a lamellar porous scaffold configuration. This unique structure facilitates the encapsulation of the liquefied PCMs, effectively preventing the leakage of PEG when temperatures rise above the melting point. The capillary forces within the porous scaffold play a crucial role in maintaining the integrity of the encapsulated material, ensuring the stability and efficiency of the PCM under thermal stress[68], [69], [70]. This design is pivotal for applications requiring thermal management, where controlled release and containment of materials at varying temperatures are essential. Further analysis was conducted using Energy Dispersive X-ray Spectroscopy (EDS) to assess the distribution of materials within the composite films. In Fig. 3, the EDS maps clearly demonstrated the homogeneous distribution of hectorite nanoparticles throughout the composite, enhancing both structural integrity and thermal properties of the film. This compositional analysis verifies the

robustness and reproducibility of the synthesis process, yielding materials with consistent and reliable qualities. The uniformity in the film's composition suggests the potential for scaling up these advanced manufacturing techniques.

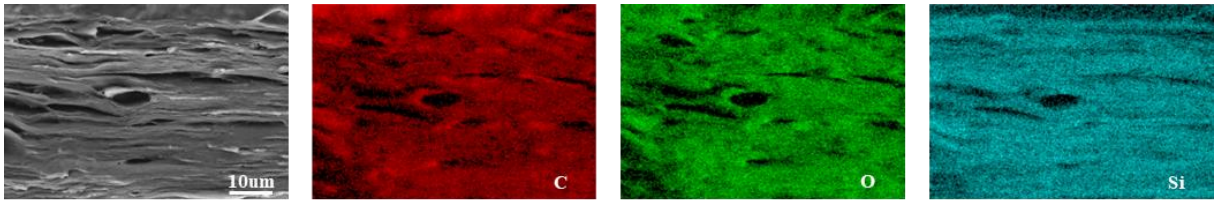

Figure 3. SEM and EDS image of the composite PEG/CNF/Hectorite15% film.

3.2.2 synthesis mechanism

To understand the synthesis mechanism of the sample, FTIR and XRD analyses were performed. FTIR analysis was used to investigate the internal interactions within the composite film samples, as shown in Fig. 4a. The FTIR spectra reveal a broad from 3700-3100 cm^{-1}, indicate the O-H group stretching vibrations, including PEG, CNF and hectorite[20], [71], [72], [73]. The notable shift to lower range in the composite film indicating the formation of intermolecular hydrogen bonding. Specific peaks at 2892 cm^{-1}, 1100 $cm^{-1,}$ and 1010 cm^{-1} in PEG are identified as C-H, C-O-C, and Si-O-Si stretching vibrations, respectively[74], [75]. CNF shows a peak at 1619 cm^{-1} for -COO- stretching [76], [77], while hectorites' characteristic peaks at 1638 cm^{-1} and 1010 cm^{-1} are associated with Si-O vibrations[78]. When crosslinked by Ca^{2+}, the CNF carboxyl peaks shift to 1600 cm-1 and 1436 cm-1, highlighting strong Ca^{2+}interactions[79]. These shifts and changes in peak intensity due to electrostatic interactions between ingredients suggest a purely physical formation process for the composite films. The fabrication involves hydrogen bonding and electrostatic interactions that form a stable, flexible 2D laminar network, enhanced by the addition of Ca^{2+} ions for increased mechanical strength, as illustrated in Fig. 1.

XRD analysis was employed to examine the crystallinity of the composite film and its precursors, with Fig. 4b displaying the XRD patterns of both the composite films and the raw materials. CNF is characterized by a broad peak at $2\theta = 22°$, which signifies its amorphous nature [80]. PEG is marked by two distinct peaks at $2\theta = 19°$ and 23° [81], whereas hectorite features two broad peaks at $2\theta = 20°$ and 35° [82]. The XRD pattern of the composite film shows the characteristic peaks of PEG alongside the amorphous background associated with CNF, indicating the coexistence of crystalline PEG and amorphous CNF within the film. After being incorporated into the composite, PEG maintained its original crystallinity, highlighting its exceptional chemical compatibility with hectorite and CNF. This presence of crystalline PEG in the composite film is crucial for ensuring the phase change performance of the materials[83], [84]. XRD analysis reveals the fusion and crystallization of PEG within the composite, which is essential for the optimal phase change performance of the PCM film.

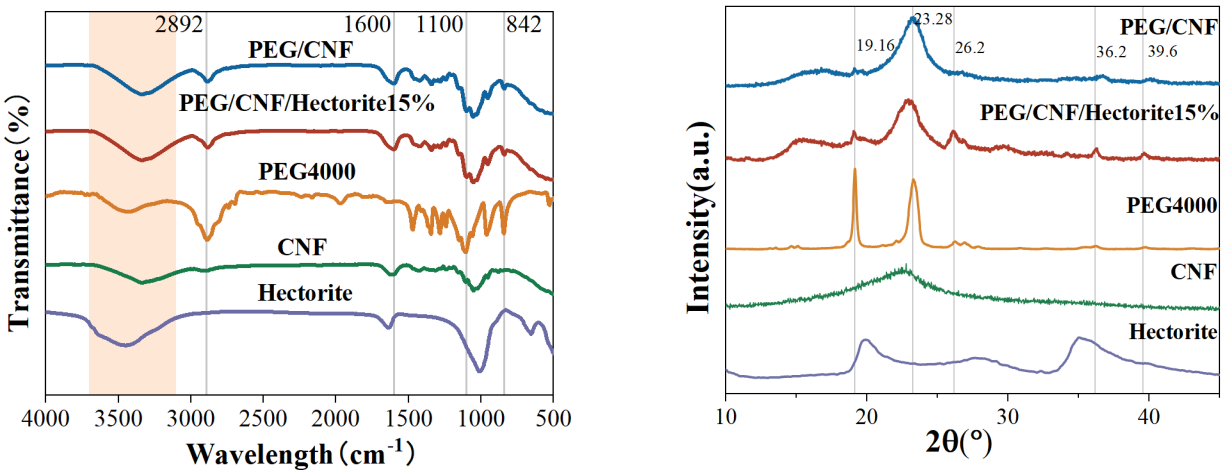

Figure 4. (a) FTIR of PEG/CNF, PEG/CNF/Hectorite15%, PEG4000, CNF, Hectorite. (b) XRD of PEG/CNF, PEG/CNF/Hectorite15%, PEG4000, CNF, Hectorite.

3.3 Study on the phase change performance

3.3.1 Latent heat performance

Phase change properties were assessed using Differential Scanning Calorimetry (DSC) for composites containing various amounts of hectorite. Fig. 5a and 5b illustrate the exothermic and endothermic DSC profiles of the composite films alongside PEG. Important data such as melting, or crystallization enthalpies are documented in Table 4. For films with 5%, 10%, and 15% hectorite, the crystallization enthalpies are 70.28 J/g, 74.30 J/g, and 79.65 J/g, respectively, and the melting enthalpies are 83.40 J/g, 95.16 J/g, and 100 J/g. These findings indicate that hectorite disrupts hydrogen bonding between PEG and CNF, likely due to a physical barrier. Additionally, to explore the adaptability of phase change temperatures, different molecular weights of PEG were used in the PEG/CNF/Hectorite15% film. Results in Table 5 show that the latent heat and enthalpies of fusion and crystallization increase with the molecular weight of PEG. Fusion enthalpies ranged from 113.2 J/g for PEG800 to 202.0 J/g for PEG4000, and up to 200.0 J/g for PEG6000. Correspondingly, fusion temperatures varied from 24.2°C (PEG800) to 59.59°C (PEG6000), and crystallization temperatures ranged from 26.19°C (PEG800) to 49.49°C (PEG6000). These adjustable phase change temperatures enable the composite films to function across different operational temperatures, enhancing their versatility for various applications.

A series of experiments was conducted using an infrared camera to analyze phase change performance in PEG/CNF/Hectorite15% and CNF films. These films were placed on an isothermal heat plate, with their temperature distributions documented in Fig. 6. During the initial heating phase, both films showed a similar rise in temperature from 10 to 30 seconds. From 30 to 50 seconds, however, the CNF film's temperature increased more significantly, reaching 64.8°C at 40 seconds and 77.8°C at 50 seconds. In contrast, the temperature of the PEG/CNF/Hectorite15%

film was lower, rising to 53.3°C at 40 seconds and 64.8°C at 50 seconds, which is 11.5°C and 13°C cooler, respectively. This highlights the composite film's enhanced heat absorption capabilities due to the heat absorption from solid to liquid phase change. For the cooling phase, the initial temperature of both films was approximately 56.3°C. The CNF film cooled quickly, dropping to 31.0°C by 50 seconds. Meanwhile, the PEG/CNF/Hectorite15% film showed a more gradual cooling curve, ending at 47.5°C at 50 seconds, which was 16.5°C higher than the CNF film. This indicates that the composite film also experienced phase change and released heat during cooling phase. Overall, the synthetic PEG/CNF/Hectorite15% films display effective phase change behavior, absorbing and releasing thermal energy efficiently during temperature fluctuations.

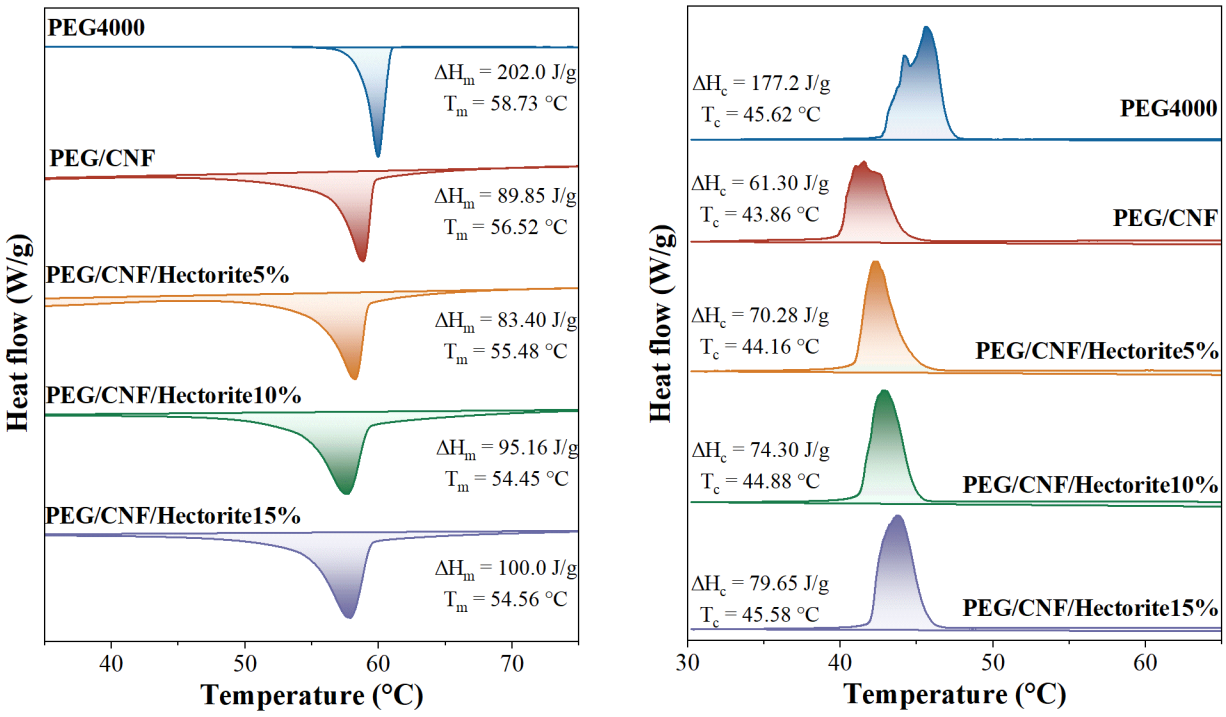

Figure 5. (a) Exothermic DSC profile and (b) endothermic DSC profile for the PEG4000, PEG/CNF, and PEG/CNF/Hectorite film.

Table 4. Phase change enthalpies and temperatures for samples made with PEG4000.

Sample	T_c(◦C)	ΔH_c(J/g)	T_m(◦C)	ΔH_m(J/g)
PEG	45.62	177.20	58.73	202.00
PEG/CNF	43.86	61.30	56.52	89.85
PEG/CNF/ Hectorite5%	44.16	70.28	55.48	83.40
PEG/CNF/ Hectorite10%	44.88	74.30	54.45	95.16
PEG/CNF/ Hectorite15%	45.58	79.65	54.65	100.00

Table 5. Phase change enthalpies and temperatures for samples with different PEG

Sample	T_c(◦C)	ΔH_c(J/g)	T_m(◦C)	ΔH_m(J/g)
PEG 800	26.19	113.20	24.20	113.20
PEG800/CNF/ Hectorite15%	25.90	58.59	21.41	73.63
PEG 4000	45.62	177.20	58.73	202.00
PEG4000/CNF/ Hectorite15%	45.58	79.65	54.65	100.00
PEG 6000	49.49	188.60	59.59	200.06
PEG6000/CNF/ Hectorite15%	46.85	93.05	58.66	99.86

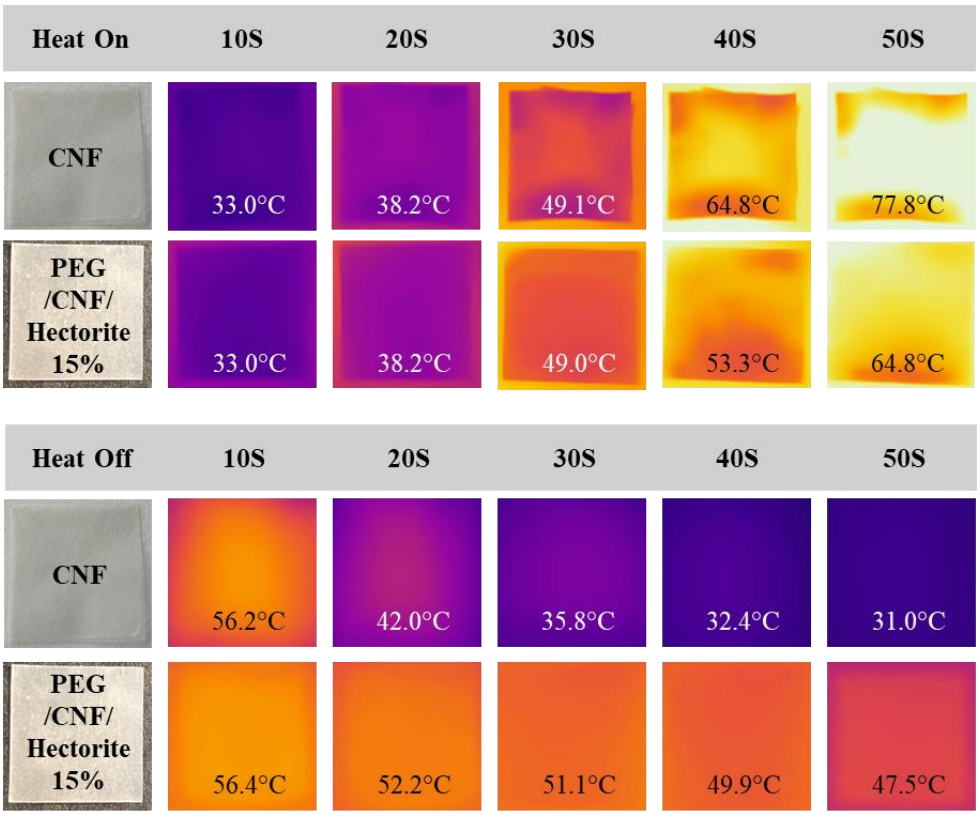

Figure 6. Infrared thermal images of CNF film and PEG/CNF/Hectorite15% film during heating and cooling.

3.3.2 Stability test

Thermogravimetric analysis was utilized to establish the effective working temperature range of the composite films, with TG curves and DTG profiles shown in Fig. 7a. The decomposition temperatures range from 201°C to 288°C for CNF and from 339°C to 431°C for PEG[85]. CNF composite films can retain some water, leading to about a 9% weight loss by 100°C [86]. The percentage of mass loss during a 30-minute exposure to 70°C on a heating board is depicted in Fig. 7b, corresponding to the TG curve for water loss within this temperature range. The degradation profile of the composite PCM films reflects a blend of CNF and PEG behaviors, decomposing in two stages: from 242°C to 316°C for CNF and from 365°C to 425°C for PEG.

This indicates thermal stability from 0°C to 242°C, encompassing PEG's phase change temperature range of 10-70°C, thus ensuring stable phase change performance of the film.

Leakage tests were meticulously carried out to assess the structural integrity of the films under thermal stress, and the results are visually documented in Fig. 8. These tests involved heating samples at 70°C for a duration of 30 mins. It was observed that the pressed PEG films, when subjected to these conditions, tend to lose their structural cohesiveness, and become liquid as they reach their fusion temperatures, demonstrating a clear alteration in physical state. In stark contrast, the PEG/CNF and PEG/CNF/Hectorite films maintained their original appearance even after the heating process. This remarkable stability can be attributed to the unique laminar porous structures formed by the integration of CNF and hectorite within the composite. These structures effectively encapsulate and retain the liquefied PEG, preventing any leakage or shape distortion at elevated temperatures. This functionality not only emphasizes the film's superior liquid encapsulation capabilities.

The durability of the synthetic films was assessed through thermal cycle stability tests on PEG/CNF/Hectorite15% films, with DSC profiles under three different conditions (original, after 20 cycles, and after 50 cycles) presented in Fig. 9a and 9b. Data recorded in Table 6 shows minimal changes in enthalpies and phase change temperatures after the test cycles, demonstrating the films' excellent durability. This durability supports up to 50 repeated heating and cooling cycles, extending the potential range of practical applications. These results collectively underscore the exceptional thermal stability and durability of the composite films under 242°C, ensuring reliable performance within PEG's adjustable fusion temperature ranges and a prolonged service life.

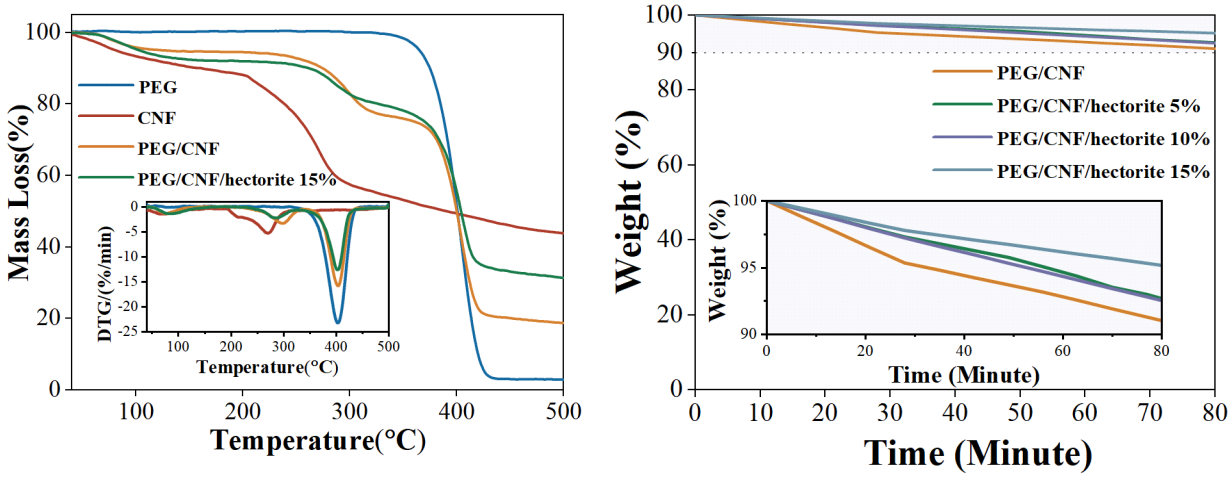

Figure 7. (a) TG and TGA profile of PEG, CNF, PEG/CNF, PEG/CNF/Hectorite15% film. (b) Weight retains percentages of composites films.

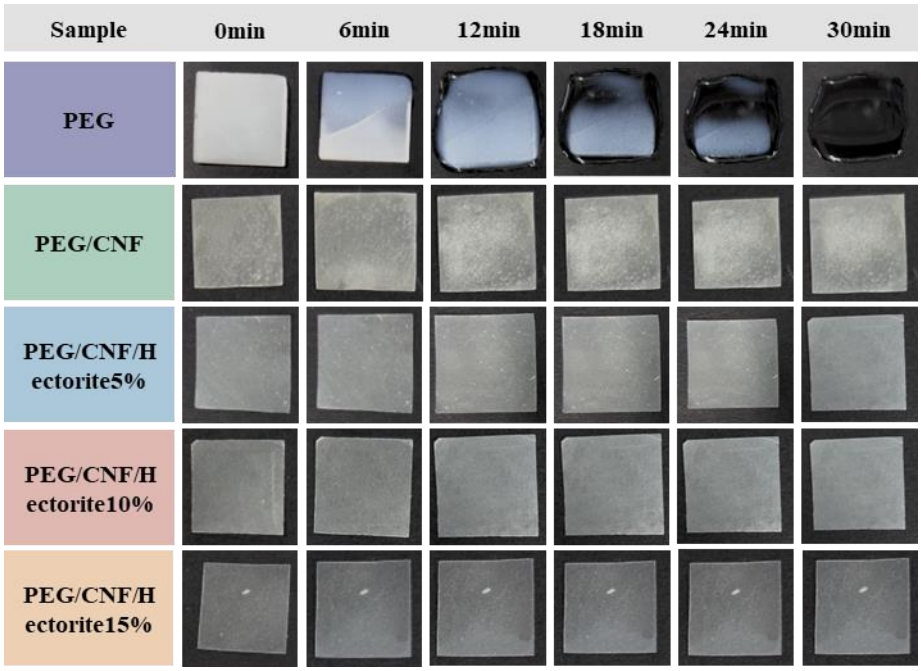

Figure 8. Shape stability test results PEG, PEG/CNF, PEG/CNF/Hectorite films.

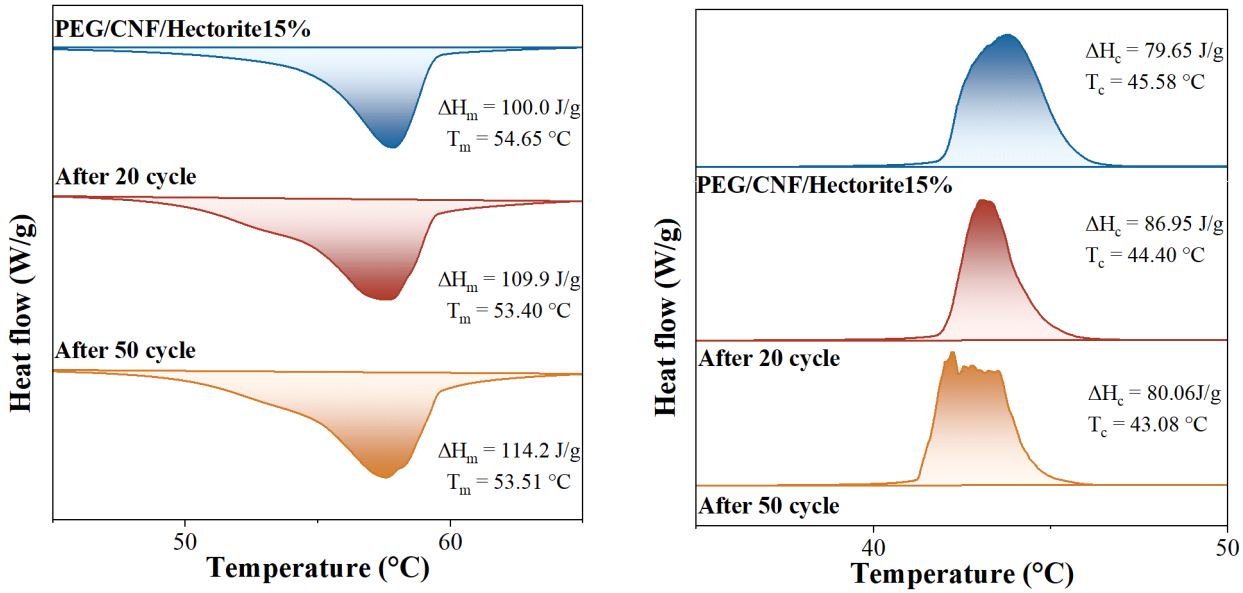

Figure 9. (a) Exothermic and (b) endothermic DSC profiles of composite PCM before and after 20/50 heating and cooling cycles

Table 6. Phase change enthalpies and temperatures for composites films before and after cooling and heating cycles.

Sample	T_c(◦C)	ΔH_m(J/g)	T_m(◦C)	ΔH_m(J/g)
PEG/CNF/ Hectorite15%	45.58	79.65	54.65	100.00
CYCLE 20	44.40	86.95	53.40	109.90
CYCLE 50	43.08	80.06	53.51	114.20

3.3.3 mechanical strength test

In the utilization of synthetic films, particularly PCM films, possessing robust mechanical properties is essential, especially when these flexible PCM films are subject to frequent mechanical stresses such as bending, stretching, or folding when applied to curved surfaces[49], [55]. The mechanical performance is critical in ensuring that the films can withstand the physical demands of their applications without failure. Fig. 10a highlights the exceptional mechanical strength of the PEG/CNF/Hectorite15% film, demonstrated by its capability to lift a 500g weight. This substantial mechanical strength enables the film to effectively handle tensions and stresses encountered during practical applications, contributing significantly to the extended service life of the films, and demonstrating the ability of maintaining their structural integrity under various mechanical stresses. The stress and strain characteristics of these films are detailed in Fig. 10c, where PEG/CNF films exhibit a tensile strength of 9.56 MPa and a fracture strain of 3.92%. However, when hectorite is incorporated into the films, there is a noticeable enhancement in mechanical properties. The addition of hectorite elevates the tensile strength to 16.84 MPa and modifies the fracture strain slightly to 3.27%. Further mechanical data, showcased in Fig. 10b, reveal that hectorite not only boosts the tensile strength and fracture strain but also significantly increases the elastic modulus from 802.24 MPa in the PEG/CNF films to 1055.26 MPa in the PEG/CNF/Hectorite15% films. This improvement in mechanical strength broadens the potential applications of the PEG/CNF/Hectorite15% films, making them more resilient to bending and stretching stresses, thus enhancing their durability in demanding environments.

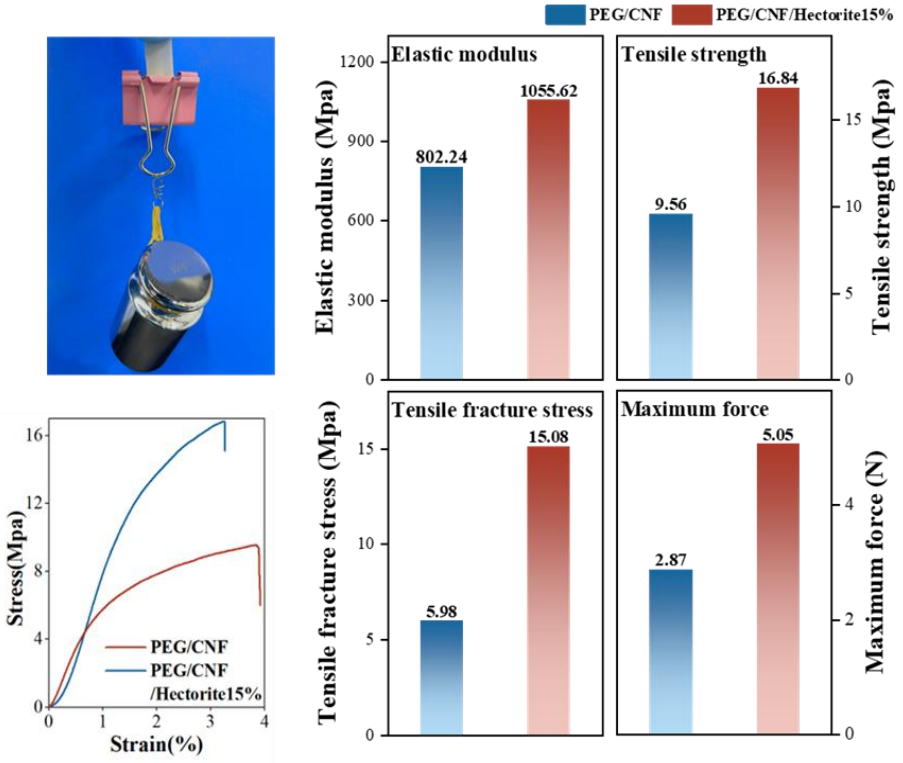

Figure 10. (a) Composite film pulling up 500g weight, (b) elastic modulus, tensile strength, tensile fracture stress and maximum force for of composite film and (c) stress and strain curve.

3.3.4 flame retardancy

One notable drawback of organic PCMs is their inherent flammability. However, the incorporation of hectorite, a non-flammable natural clay mineral, has been shown to mitigate this risk significantly in composite films[87], [88]. To evaluate the flammability of these films, a series of experiments were conducted on PEG/CNF and PEG/CNF/Hectorite15% films. The heat release rate (HRR) profiles, recorded at various temperatures, are displayed in Fig. 11. Both profiles exhibit two peaks: the first ranging from 247°C to 322°C, during which the PEG/CNF film releases 35.1W/g and the PEG/CNF/Hectorite15% film releases 19.5W/g; the second peak ranges from 351°C to 460°C, with the PEG/CNF film emitting 368.5W/g and the PEG/CNF/Hectorite15% film 304.5W/g. These peaks correspond to the decomposition of CNF and PEG, respectively, as confirmed by previous TG test results. In both cases, the films reinforced with hectorite exhibited lower heat release rates compared to those without hectorite. Additional data from Micro Calorimeter Cone (MCC) tests showed that the specific heat capacity was 380J/g·K for the PEG/CNF film and 313J/g·K for the PEG/CNF/Hectorite15% film. Total heat release was 14.3KJ/g for the PEG/CNF film and 12.9KJ/g for the PEG/CNF/Hectorite15% film, indicating enhanced resistance to flammability in the hectorite-enhanced composite film.

Complementary to the MCC test results, digital camera footage captured the burning process of both film sets under vertical and horizontal conditions, as shown in Fig.12a. During these tests, the PEG/CNF/Hectorite15% films exhibited a delayed ignition time compared to the PEG/CNF films. Post-combustion residues, depicted in Fig. 12b, reveal that while the PEG/CNF films shrank and deformed, the PEG/CNF/Hectorite15% films maintained nearly their original shape with a smooth surface. This demonstrates that in the event of a fire, PEG/CNF/Hectorite15% films are capable of preserving their structural integrity, thereby offering protection to the underlying application surfaces, thus reducing environmental damage. These results highlight the significant flame-retardant properties of the synthetic flexible films granted by hectorite, underscoring the hectorite's ability to enhance the films' structural resilience during thermal events.

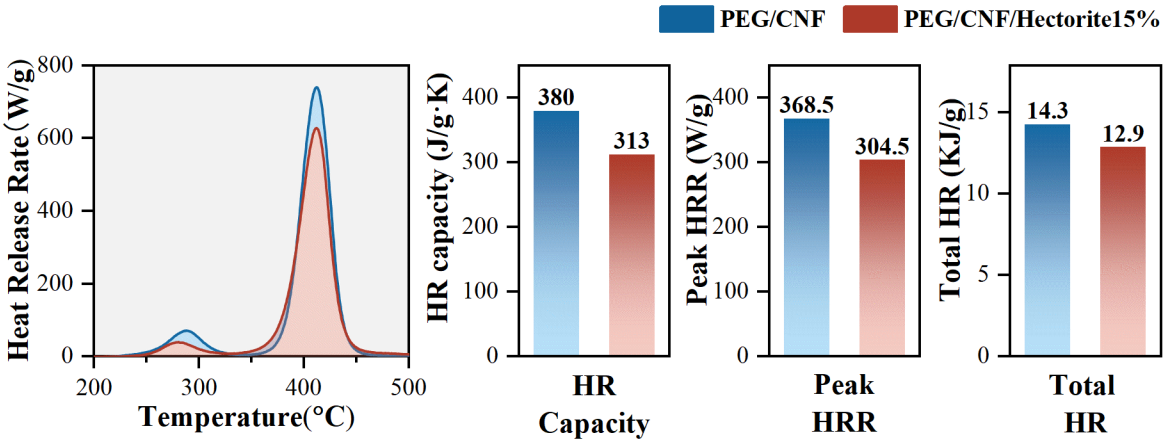

Figure 11. HRR vs. temperature curves, heat release capacity, peak HRR, and total heat release of samples.

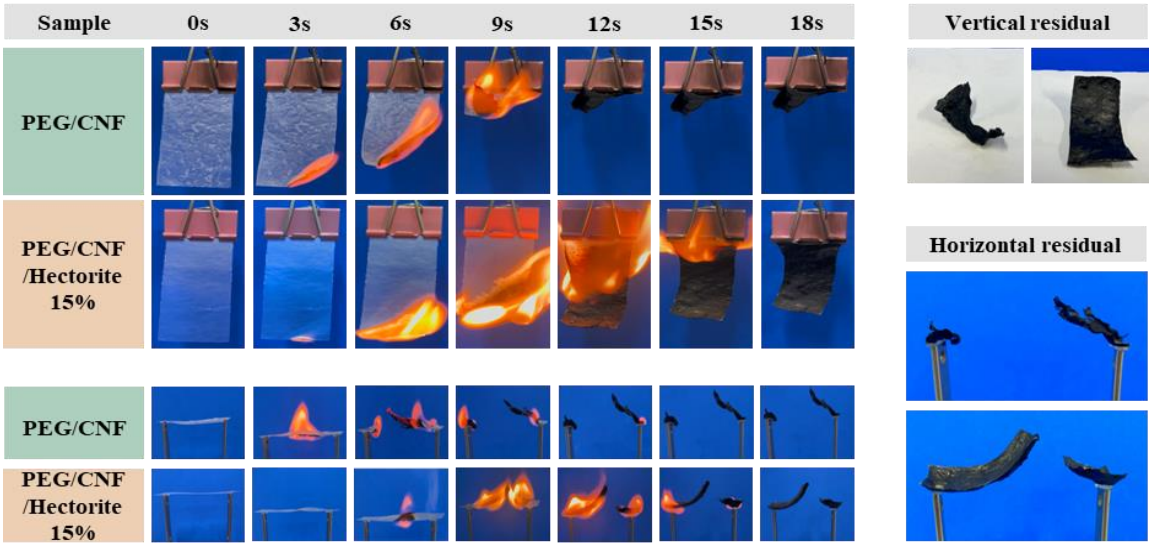

Figure 12. (a) Digital images of the films subjected to vertical and horizontal burning conditions. (b) Residual images post-burning showing the PEG/CNF film (top-left, middle) and the PEG/CNF/Hectorite15% film (top-right, bottom).

3.4 Conclusion

In this study, hectorite is identified as a key component in the development of a flexible PCM film that also includes PEG and CNF. The inclusion of hectorite not only significantly enhances the film's mechanical strength but also serves as an effective flame retardant. This dual functionality of hectorite greatly increases the structural integrity and fire resistance of the material. For instance, PEG/CNF films without hectorite exhibit a tensile strength of 9.56 MPa and a fracture strain of 3.92%. However, the incorporation of hectorite into the films boosts the tensile strength to 16.84 MPa while slightly modifying the fracture strain to 3.27%. This enhancement in mechanical properties such as tensile strength and elasticity makes the film more durable and robust for practical applications. These improved mechanical characteristics are particularly valuable for extending the film's use in sectors like wearable thermal management, flexible electronics, and green building design, where both mechanical strength and safety are crucial.

4. Graphene enhancing heat conductivity and photothermal properties in PCM film

4.1 Method

The graphene nanoplates(GNP) enhanced phase change film was produced using the following procedures, with water serving as the solvent. Initially, specific proportions of PEG and

GNP were combined in a beaker filled with a measured volume of pure water. This blend was magnetically stirred at 500 rpm for 60 mins to ensure complete dissolution and uniform distribution. Following this dispersion phase, a predefined quantity of CNF was added to the mixture, which was then processed in a high shear emulsification machine at 16000 rpm for 15 mins. Subsequently, the mixture was degassed under vacuum for 15 mins before being poured into a polytetrafluoroethylene mold to facilitate a 12-hour crosslinking process. Afterwards, the resulting hydrogel was immersed in a 1 wt.% calcium chloride solution for 10 mins to enhance crosslinking and then thoroughly washed with deionized water. The gel was allowed to air dry at room temperature for 48 hours. A schematic of this synthesis process is illustrated in Fig. 13, with the various percentages of components specified in Table 7.

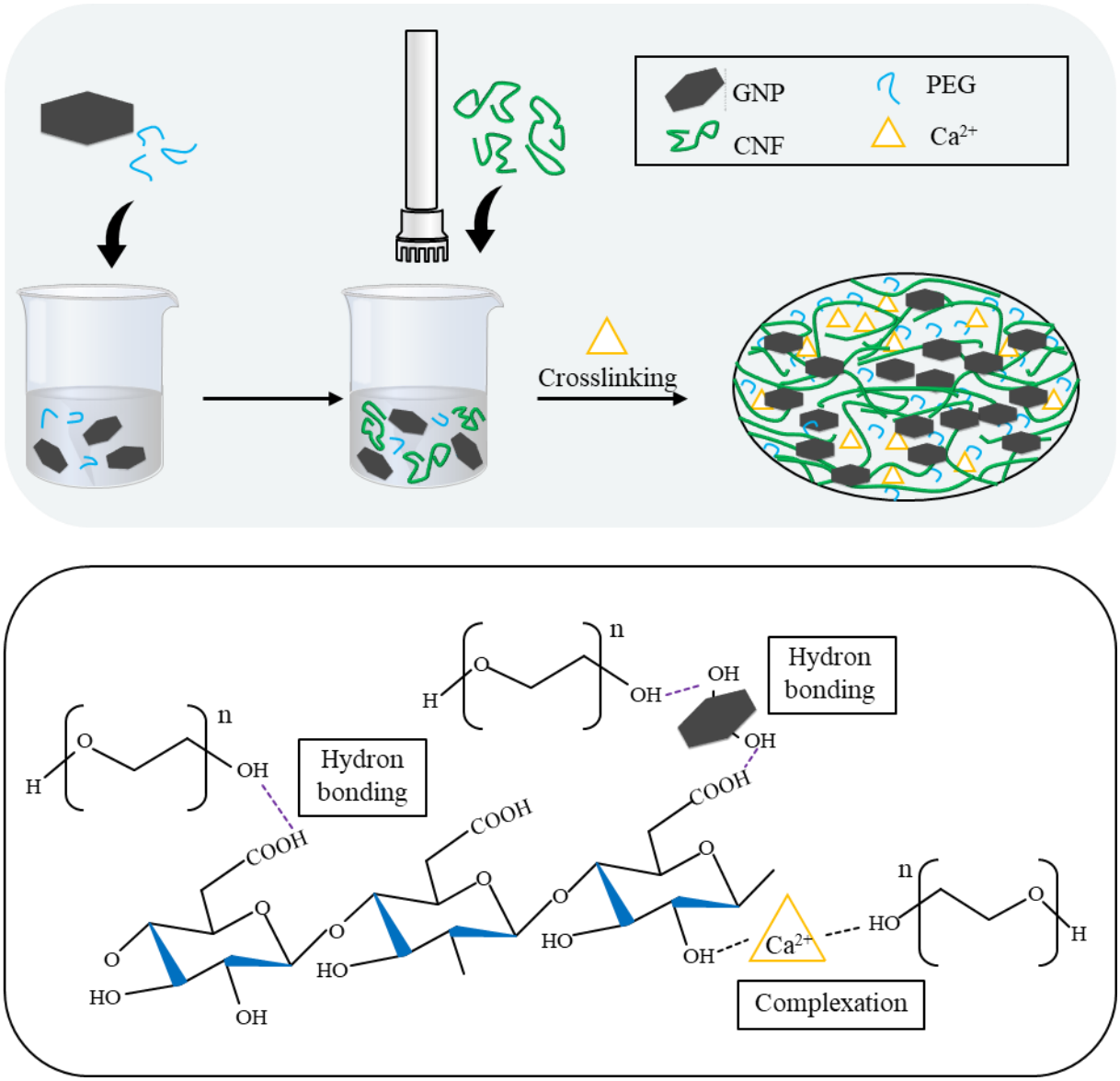

Figure 13. Schematic diagram for synthesizing PEG/CNF/GNP composite flexible PCM.

Table 7. Sample composition ratios for GNP enhanced PCM film.

Sample name	PEG (wt%)	CNF (wt%)	GNP (wt%)
PEG/CNF	70	30	0%
PEG/CNF/GNP5%	70	25	5
PEG/CNF/GNP10%	70	20	10
PEG/CNF/GNP15%	70	15	15

4.2 Characteristics and synthesis mechanism

4.2.1 Characteristics

This section presents a detailed examination of both the macroscopic observations and the microscopic features of the GNP enhanced PCM film. From a macroscopic perspective, digital photographs in Fig. 14a and 14b illustrate the flexibility and structural integrity of the GNP-enhanced PCM films at different scales. Fig. 14a displays a small-sized (2 x 2 cm) PCM film bent to demonstrate its flexibility, while Fig. 14b shows a larger-sized (15 x 15 cm) bent film, further highlighting the material's adaptability and its potential for large-scale manufacturing applications. Microscopically, the film's morphological structure is revealed through Scanning Electron Microscopy (SEM) analysis shown in Fig. 14c. The SEM image showcases a lamellar porous scaffold structure within the PEG/CNF/GNP15% films, reminiscent of the structure observed in PEG/CNF/hectorite films. This specific architecture is crucial as it effectively encapsulates the liquefied PEG, preventing any leakage during the phase change process. The detailed lamellar structure not only contributes to the film's mechanical stability under thermal stress but also enhances its functional performance by ensuring a consistent and controlled release of thermal energy. Additionally, the lamellar structure allows the film to retain its flexibility, enabling it to bend and deform without compromising its overall integrity[89]. This combination of flexibility at the macro level and robust structural configuration at the micro level underscores the composite film's suitability for diverse applications, from wearable technologies to energy-efficient building materials.

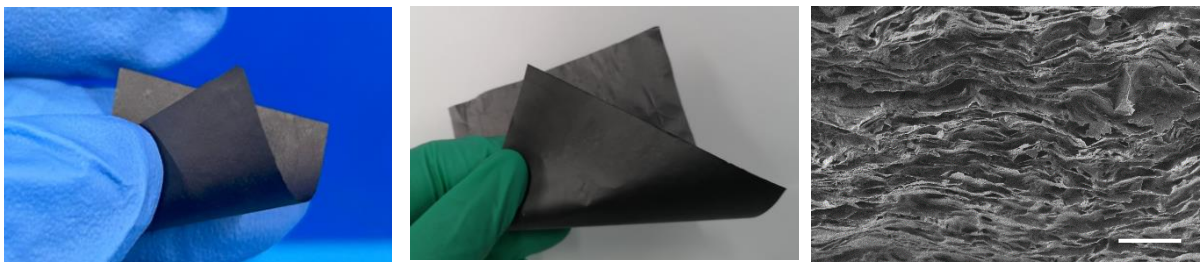

Figure 14. Digital photo of the composite PEG/CNF/GNP15% film samples (a) bended, (b) large sized sample bended. SEM image of the PEG/CNF/GNP15% film.

4.2.2 synthesis mechanism

To elucidate the synthesis mechanism and the interactions within the composite film samples, FTIR analysis was conducted, as illustrated in the Fig. 15a. The FTIR spectra for GNP spectrum show relatively low transmittance with fewer distinct peaks, typical of graphene-based materials which often exhibit less pronounced IR-active vibrations[90], [91]. CNF displays a significant peak around 1600 cm^{-1}, indicative of C=O stretching vibration from carboxylic groups[92], [93]. PEG's spectrum reveals key peaks at 2892 cm^{-1} for C-H stretching and 1100 cm^{-1} for C-O-C ether vibrations, underlining the structural backbone of PEG that contributes to the phase change properties[94], [95]. The composite spectrum merges these features but shows shifts, the broad band from 3500-3000 cm^{-1} indicating O-H group stretching, representing intermolecular hydrogen bonding during synthesis[96], [97]. The observed spectral changes highlight the successful incorporation of GNP, optimizing the film's functionality for robust thermal management and mechanical applications, confirming the intended synthesis strategy and the synergistic interaction between PEG, CNF, and GNP within the developed composite.

The X-ray diffraction (XRD) spectrum (Fig. 15b) reveals the crystalline structures of GNP, cellulose nanofibrils (CNF), polyethylene glycol (PEG), and their composite, PEG/CNF/GNP15%. GNP shows a sharp peak at around 26.5°, sharing the same peak with GNP, typical of its graphitic crystalline structure[98]. CNF, which is more amorphous, displays a broader and less intense peak, usually seen around 22° [99], [100], [101]. PEG4000, identified by its semi-crystalline nature, exhibits clear peaks at 19.16° and 23.28° [95]. In the composite, these characteristics overlap, showing that the distinct properties of each material are preserved. The sharp peak from GNP and the specific peaks from PEG suggest that their crystalline attributes remain intact within the composite. This indicates that the functional qualities of GNP's mechanical strength and PEG's phase change capabilities are maintained, enhancing the composite's overall performance. The retention of these peaks in the composite also points to good compatibility among the materials, suggesting their effective integration without significant structural disruption.

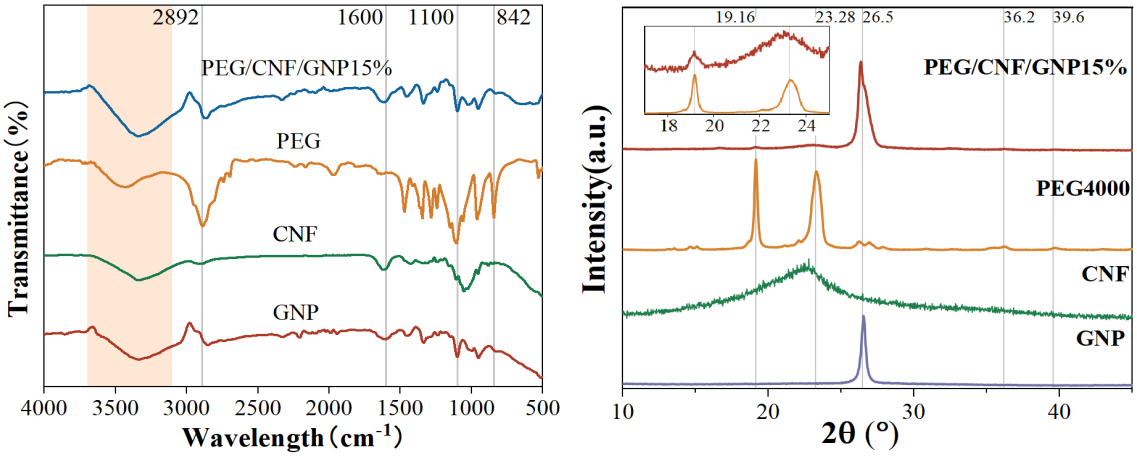

Figure 15. (a) FTIR of PEG/CNF, PEG/CNF/GNP15%, PEG4000, CNF, GNP. (b) XRD of PEG/CNF/GNP15%, PEG4000, CNF, GNP.

4.3 Study on the phase change performance

4.3.1 Latent heat performance

The Differential Scanning Calorimetry (DSC) results displayed in Fig. 16a,b and data recorded in Table 8 reveal a promising trend in enhancing thermal properties with the incremental addition of graphene to the PEG/CNF composite. The base PEG/CNF film, characterized by a crystallization enthalpy of 61.30 J/g and a temperature of 43.86°C, sees notable improvements with the introduction of graphene. When 5% graphene is added, the crystallization enthalpy slightly increases to 63.65 J/g, and the temperature moderately reduces to 39.68°C, suggesting an enhanced thermal stability. This positive trend continues with the PEG/CNF/Graphene10% composite, which shows a further increased crystallization enthalpy of 67.14 J/g and a reduced temperature of 40.95°C, indicating improved energy storage capacity and thermal efficiency. The exothermic melting transitions also reflect a similar pattern; the PEG/CNF film initially exhibits a melting enthalpy of 89.85 J/g and a temperature of 56.52°C. With 5% graphene, the melting enthalpy adjusts to 75.76 J/g at a temperature of 56.57°C, and the PEG/CNF/Graphene10% records a slightly higher enthalpy of 83.16 J/g at a similar temperature of 57.67°C, maintaining stability in heat absorption capabilities. However, the PEG/CNF/Graphene15% composite marks a deviation from this trend, with both crystallization and melting properties showing reductions. The crystallization enthalpy drops to 75.17 J/g and the temperature further decreases to 37.45°C, while the melting enthalpy falls to 80.12 J/g at a significantly lower temperature of 50.70°C. This indicates that beyond a certain threshold, additional graphene may compromise the thermal performance, suggesting the need for careful optimization of graphene content to ensure a balance between enhancement and material stability. As discussed in the third chapter, altering the average molecular weight of PEG allows for tuning the fusion and crystallization temperatures. This adaptability enables the films to meet diverse thermal management requirements across a range of temperatures. Such flexibility broadens potential applications, making these composites suitable for uses for various conditions.

Infrared thermal imaging was utilized to assess the phase change behavior of CNF, PEG/CNF, and PEG/CNF/GNP 15% films, as depicted in Fig. 17. The study involved tracking their temperature profiles during a controlled heating session followed by a cooling phase, yielding crucial insights into the phase change properties and thermal conductivity of these composites. Initially, all films were at an ambient temperature of 31.0°C. During the heating cycle, at 30 seconds, the temperature of the CNF film rose sharply to 58.1°C, whereas the PEG/CNF and PEG/CNF/GNP 15% films increased more gradually to 51.7°C and 49.3°C, respectively. By 60 seconds, the temperatures were 58.1°C for CNF, 51.7°C for PEG/CNF, and 49.3°C for PEG/CNF/GNP 15%. The CNF film heated the fastest, followed by PEG/CNF, and then PEG/CNF/GNP 15%. This pattern is attributed to the phase change occurring in the PEG within the composites and the addition of GNP, which efficiently manages thermal energy absorption—a key feature for applications needing controlled heat uptake. From 60 to 120 seconds, the temperature of the PEG/CNF film rose from 53.4°C to 58.2°C, while the PEG/CNF/GNP 15%

film heated from 51.5°C to 61.6°C. The sharper increase in temperature for the PEG/CNF/GNP 15% film after the initial phase change phase highlights its superior thermal conductivity, enhanced by the presence of GNP. This property is crucial for scenarios requiring a rapid yet regulated thermal response. During the cooling process, the PEG/CNF/GNP 15% film cooled more slowly than the others, settling at 28.5°C after 60 seconds, compared to 25°C for CNF and 25.1°C for PEG/CNF. This slower cooling rate underscores the film's ability to retain heat for extended periods, showcasing the composite's excellent phase change properties. This enhanced thermal retention further exemplifies the films' potential for diverse thermal management applications. Overall, the synthetic PEG/CNF/Hectorite15% films exhibit proficient phase change performance, effectively absorbing and dissipating thermal energy in response to temperature variations.

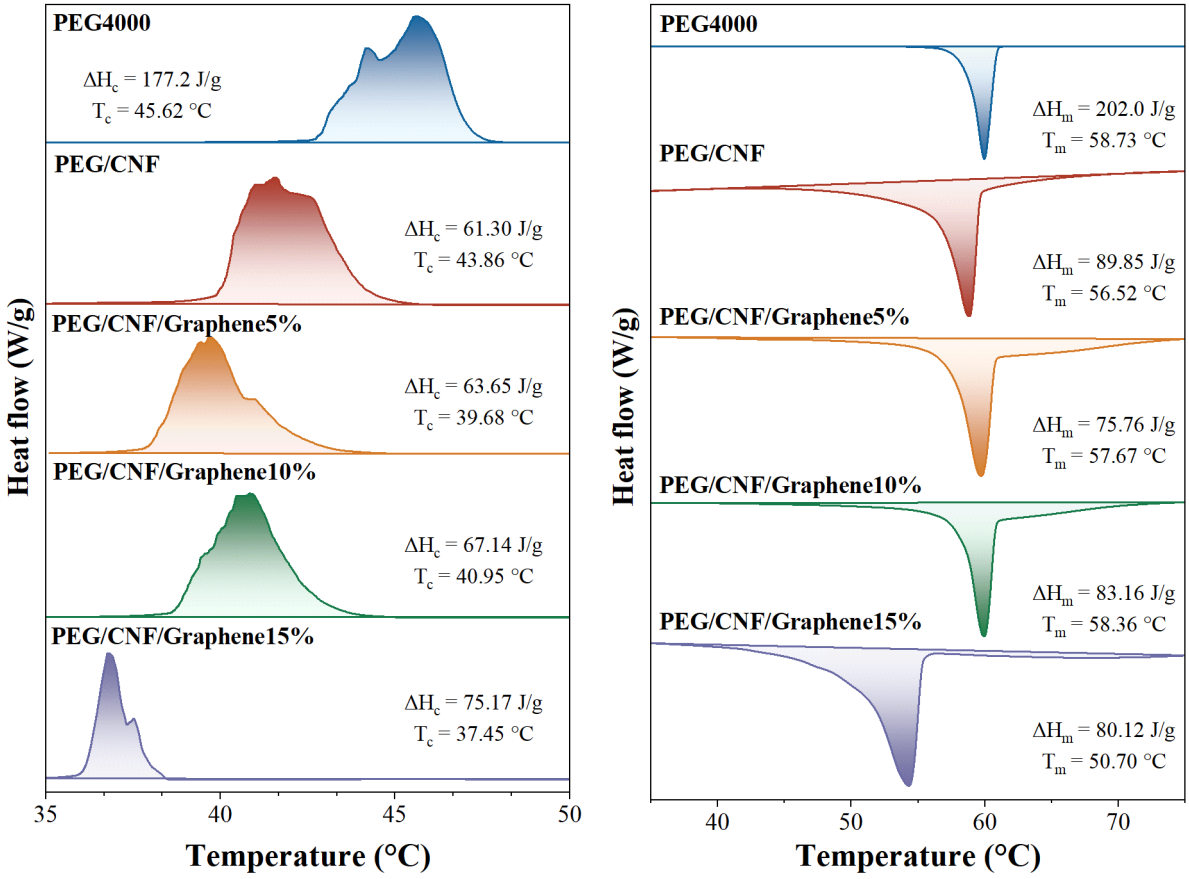

Figure 16. (a) Exothermic DSC profile and (b) endothermic DSC profile for the PEG4000, PEG/CNF, and PEG/CNF/GNP film.

Table 8. Phase change enthalpies and temperatures for samples made with PEG4000 and GNP.

Sample	T_c(◦C)	ΔH_c(J/g)	T_m(◦C)	ΔH_m(J/g)
PEG	45.62	177.20	58.73	202.00
PEG/CNF	43.86	61.30	56.52	89.85
PEG/CNF/ GNP5%	39.68	63.65	57.67	75.76
PEG/CNF/ GNP10%	40.95	67.14	58.36	83.16

PEG/CNF/ GNP15%	37.45	75.17	50.70	80.12

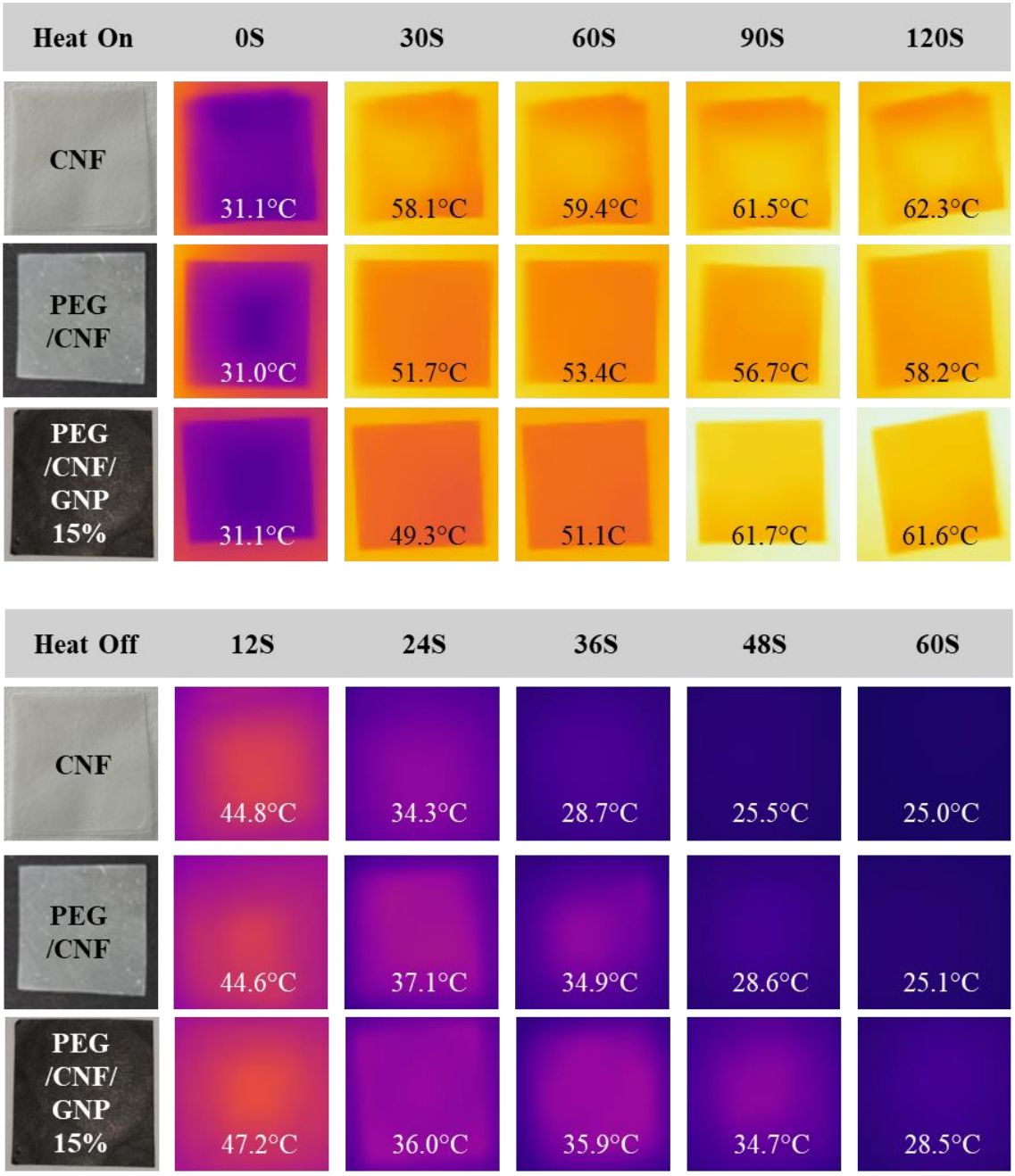

Figure 17. Infrared thermal images of CNF, PEG/CNF and PEG/CNF/GNP15% films during heating and cooling.

4.3.2 thermal stability

TGA was utilized to determine the effective working temperature range of various composite films, as presented in the TG curves and DTG profiles of Fig. 18a. This analysis provides insight into the thermal stability and decomposition characteristics of the materials

including CNF, PEG, PC, GNP, and the PEG/CNF/GNP 15% composite. For CNF, the decomposition begins at approximately 201°C and concludes around 288°C[71]. Notably, CNF retains some moisture, contributing to about a 9% weight loss by 100°C, evident during a 30 mins exposure at 70°C on a heating board, aligning with the observed TG curve for water loss, showing similar behaviors have the hectorite films. In contrast, PEG shows greater thermal stability, with decomposition initiating around 339°C and extending up to 431°C[72]. The GNP has similar TGA curve with the PEG/CNF/GNP 15%. The PEG/CNF/GNP 15% composite exhibits a more complex, two-stage decomposition process: the first stage, influenced by CNF and GNP, spans from 242°C to 316°C, and the second stage, dictated by PEG and GNP, ranges from 365°C to 425°C.This TGA and TG analysis indicates that the composite maintains thermal stability from 0°C to 242°C, effectively covering PEG's phase change temperature range of 10°C to 70°C. Therefore, the PEG/CNF/GNP 15% composite demonstrates the fit operational temperature range up to 242°C. The data in Fig. 18b illustrates moisture loss in PEG/CNF composites with varying concentrations of GNP, subjected to a steady heating temperature of 70°C. The baseline PEG/CNF composite shows the highest moisture loss, while the addition of GNP enhances moisture retention, most notably in the PEG/CNF/GNP15% composite. This demonstrates thermal stability from 0°C to 242°C, which includes PEG's phase change temperature range of 10-70°C, ensuring stable phase change performance of the film.

Leakage tests critically evaluated the structural integrity of various PEG-based composite films under thermal stress, with the documented results shown in Fig. 19. These tests were conducted by heating the samples at 70°C for 30 mins. The pure PEG film displayed rapid degradation; beginning to deform significantly at the 6-minute mark and completely liquefying by the 30-minute point, demonstrating a clear transition from solid to liquid due to thermal instability. Conversely, the composite films incorporating CNF and various concentrations of GNP (5%, 10%, and 15%) retaining its original form without any signs of melting or distortion, exhibited exceptional thermal resistance and leakage prevention. These findings highlight the potential of GNP-enhanced PEG/CNF composites for applications demanding materials that are both thermally stable and structurally reliable.

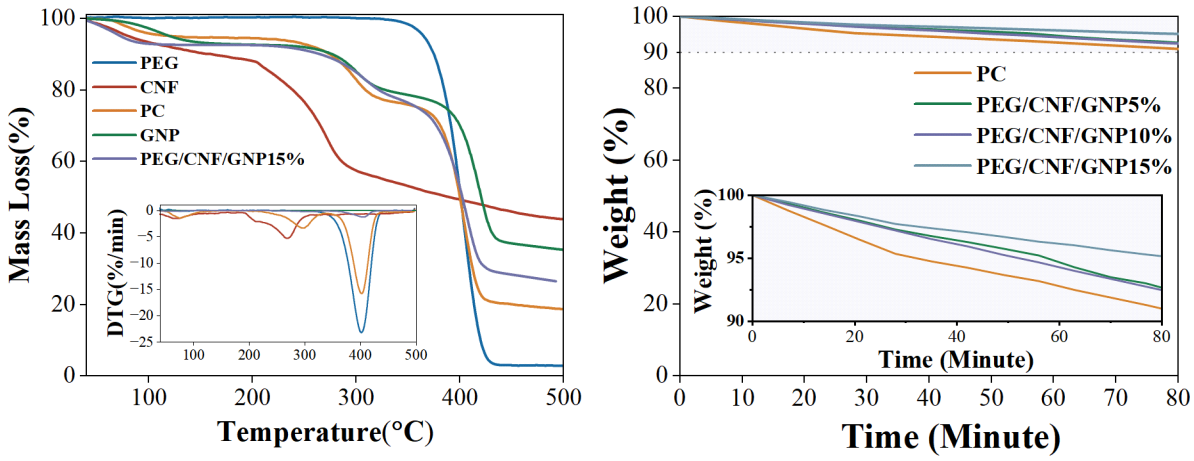

Figure 18. (a) TG and TGA profile of PEG, CNF, PEG/CNF, PEG/CNF/GNP15% film. (b) Weight retains percentages of composites films after heating.

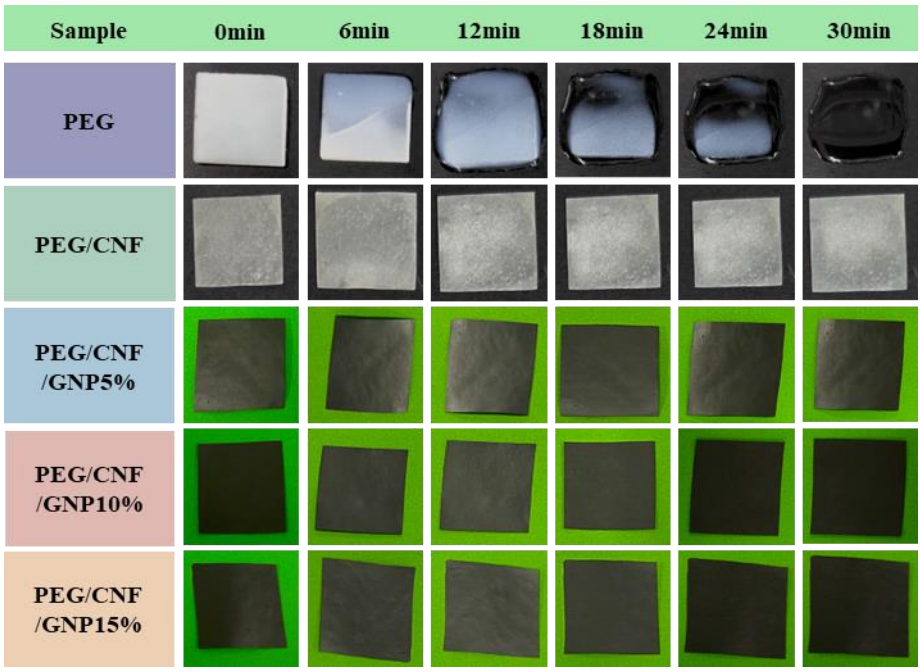

Figure 19. Digital photos of GNP enhanced samples within 30 mins of heating.

4.4 heat conductivity property

In order to test the heat conductivity for the composite films, the hot disks test was conducted. And the heat conductivity coefficients for various composite films, as shown in Fig. 20, indicate a significant variance across different formulations. Starting with the base composite of PEG/CNF, it exhibits a thermal conductivity coefficient of 0.184 W/mK. When 5% GNP are added, there is a substantial increase to 3.22 W/mK. This upward trend in thermal conductivity continues with higher GNP concentrations; the PEG/CNF/GNP10% achieves a coefficient of 11.3 W/mK, and the PEG/CNF/GNP15% further rises to 12.2 W/mK. Notably, the highest content

measured, PEG/CNF/hectorite15% made in the last chapter, reaches an way lower coefficient of 1.64 W/mK. This is because hectorite as an inorganic clay mineral does not have excellent thermal conductivity, while graphene as a semiconductor has very high thermal conductivity. Graphene has a very high thermal conductivity and thermal radiation coefficient, the thermal conductivity of single-layer graphene can reach 3000 – 5000 W/mK, which is not only better than carbon nanotubes, but also much higher than the highest thermal conductivity of metal silver, copper, gold, aluminum, etc., so graphene as a thermal conductive plastic or diaphragm to assist heat dissipation has great application prospects [102]. This progressive increase in thermal conductivity can be attributed to the exceptional thermal properties of GNP, which efficiently facilitates heat transfer within the composite laminar matrix. The addition of GNP enhances the thermal pathways available within the composites, allowing for more effective heat dissipation. These findings underscore the effectiveness of GNP in enhancing the thermal properties of PEG/CNF composites. The marked improvement in thermal conductivity with increasing GNP content demonstrates the potential of these materials for applications that demand efficient heat management.

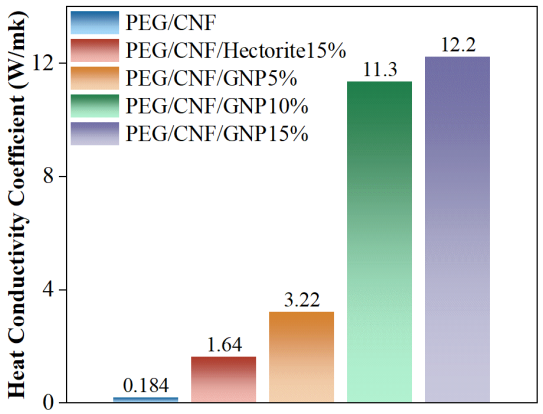

Figure 20. Heat conductivity coefficient for composite GNP films.

4.5 photothermal properties

Photothermal properties are crucial for flexible films, particularly in applications where controlled transformation of light into heat is necessary, such as in solar energy harvesting or adaptive clothing[103], [104]. To accurately assess these photothermal characteristics, films are subjected to heating under a xenon lamp, which simulates sunlight and provides a consistent source of light energy, allowing for the evaluation of the material's thermal response in real-world conditions. Fig. 21 provides a detailed visualization of the temperature profiles for CNF and PEG/CNF/GNP15% films under periodic photothermal testing. This graph distinctly showcases the phase change dynamics of the films, characterized by the sudden and significant temperature variations occurring amidst the overall heating and cooling cycles. The graph illustrates multiple cycles where both films experience rapid temperature increases followed by equally rapid cooling. However, the PEG/CNF/GNP15% composite exhibits a more pronounced stability and higher peak temperatures during these cycles compared to the CNF film. During the heating phases

(highlighted in blue), the PEG/CNF/GNP15% film consistently shows a steeper temperature rise to peak levels, suggesting an improved photothermal conversion efficiency. This is likely due to GNP's excellent thermal conductivity, which facilitates quicker heat absorption and distribution throughout the composite. Following the peak, the temperature drop is also more abrupt with the phase change bump at the crystalline temperature, demonstrating the film's ability to release stored heat efficiently, a critical feature for applications requiring rapid thermal adaptation.

In order to vividly show the temperature change in a digital photo, infrared camera was employed. Fig. 22 presents infrared imaging data illustrating the temperature progression of various films—PEG, PEG/CNF, CNF, and three grades of PEG/CNF/GNP composites (5%, 10%, 15% GNP)—heated under a xenon lamp, all starting from the same ambient temperature. The images capture the thermal response of these materials over a period from 0 to 60 seconds, showing how temperature evolves under photothermal influence. Initially, all samples are at ambient temperature, but they exhibit different heating rates once exposed to the xenon lamp. By 12 seconds, the PEG film's temperature rises modestly to 24.9°C, demonstrating a gradual increase to 30.1°C by 60 seconds. This highlights PEG's moderate photothermal responsiveness. The PEG/CNF composite shows a more pronounced initial increase, reaching 31.4°C at 12 seconds and further ascending to 36.5°C by 60 seconds. This suggests that the addition of CNF enhances the film's ability to absorb and convert photothermal energy compared to pure PEG. CNF alone displays a significant temperature rise early on, starting from the same ambient temperature and escalating to 29.7°C by 12 seconds, eventually reaching 42.4°C by 60 seconds. This indicates a higher inherent photothermal efficiency of CNF.

For the composites with GNP, the PEG/CNF/GNP 5% composite exhibits a rapid initial heat absorption, reaching 41.5°C at just 12 seconds, but its temperature rise then decelerates, achieving only 45.5°C by 60 seconds. The PEG/CNF/GNP 10% and 15% composites similarly show high initial temperatures of 42.5°C and 42.9°C at 12 seconds, respectively. However, despite these robust starting points, their temperature increases remain comparatively modest, with the PEG/CNF/GNP 15% composite peaking at 52.4°C. This moderated rate of temperature increase beyond the initial rapid heating can be attributed to the PCMs embedded within the films, which absorb significant amounts of heat during their transition, effectively modulating the overall temperature rise. The phase change impact is markedly evident in the GNP-enhanced films, where GNP's superior thermal conductivity not only facilitates rapid heat distribution across the film but also contributes significantly to the initial photothermal efficiency. This allows the films to reach higher temperatures quickly under photothermal exposure. Simultaneously, the PCMs within these composites utilize this heat energy to undergo endothermic phase transitions, which tempers any further rapid temperature escalation. This dynamic showcases the dual benefit of GNP: boosting the film's photothermal properties by enhancing initial heat absorption and dispersion, while also synergizing with PCMs to control and stabilize the temperature increase. This balanced thermal behavior underscores the potential of GNP-enhanced films for advanced applications where efficient heat management and stability are crucial.These observations underline the effective use

of GNP not only to enhance the initial photothermal response due to its superior thermal conductivity but also to moderate the overall temperature rise through synergistic phase change dynamics. This behavior is critical for applications that demand quick thermal response without overshooting desired temperature limits, making these composites ideal for sophisticated thermal management systems.

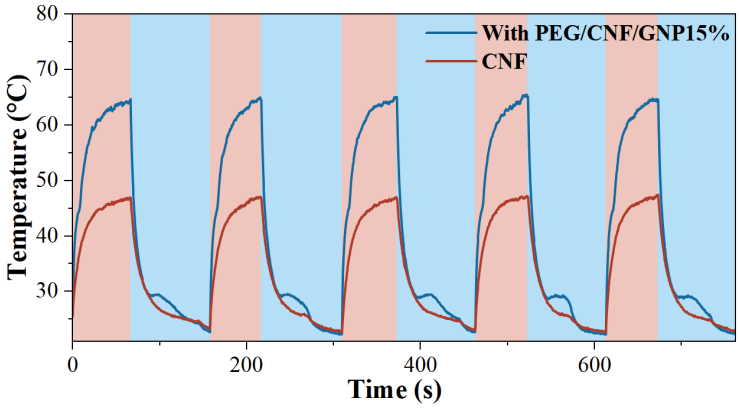

Figure 21. Temperature profile for CNF and PEG/CNF/GNP15% films during Xenon light heating and cooling cycle

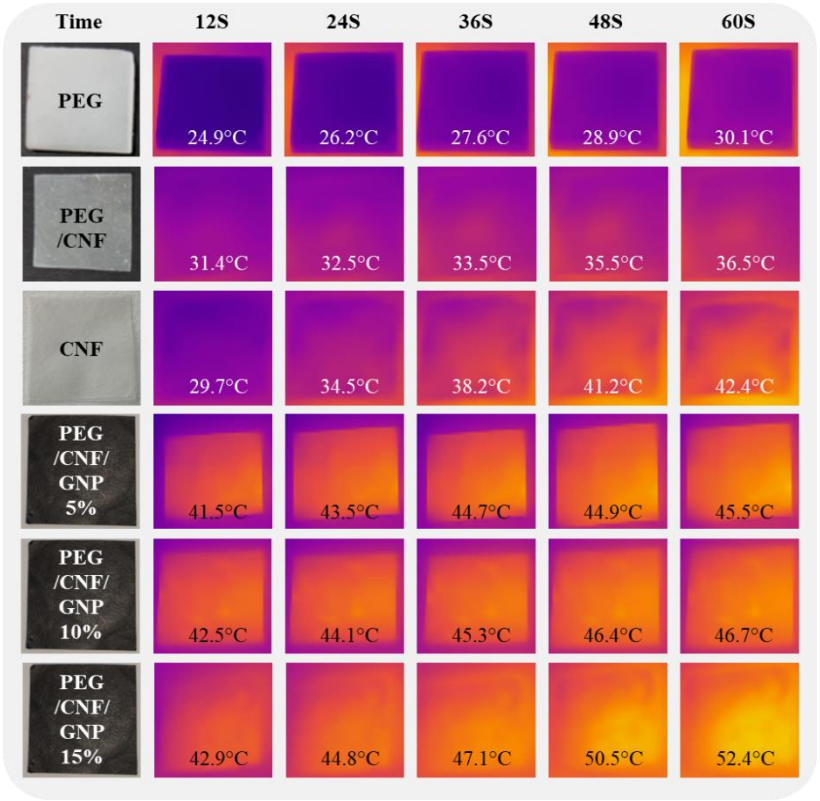

Figure 22. Infrared images for different films heating under Xenon light.

4.6 Conclusion

In this study, GNP are identified as a pivotal component in the development of flexible PCM films that also include PEG and CNF. The inclusion of GNP not only significantly boosts the film's photothermal properties but also enhances its thermal conductivity. This dual functionality of GNP considerably improves the thermal responsiveness and efficiency of the material. The addition of GNP increases the thermal conductivity of PEG/CNF composites from a base value of 0.184 W/mK to 3.22 W/mK with 5% GNP, escalating to 12.2 W/mK with 15% GNP. This dramatic improvement showcases the exceptional thermal properties of GNP, making it highly effective for advanced thermal management applications. The enhanced films exhibit superior heat absorption and distribution capabilities, as evidenced during photothermal testing with a xenon lamp, where GNP-enhanced films reached higher temperatures more rapidly compared to those without GNP. These findings underline the potential of GNP-enhanced PCMs to significantly improve the efficiency of thermal regulation technologies across various industries, from aerospace to consumer electronics, making them pivotal for future advancements in energy-efficient materials.

5. Practical applications

Practical applications are crucial for transforming theoretical research on PCM films into tangible industry solutions[49], [55]. These films are essential in energy storage, building management, textiles, and electronics for their ability to regulate temperature efficiently. In this chapter, the real-world uses of PCM films will be explored, demonstrating their versatility and effectiveness across various sectors. By highlighting specific case studies, aiminf to showcase the significant impact and commercial viability of PCM films in solving complex thermal management challenges. This discussion will bridge the gap between research and practical implementation, underscoring the potential of PCM films to revolutionize thermal regulation technologies.

5.1 Methods

5.1.1 Simulation house application experiment design

To investigate the application of PCM films in green building scenarios, a controlled experimental setup involving simulated houses was developed, and the illustration figure is demonstrated in Fig. 23 a. This experiment involved constructing two identical model houses equipped with thermal insulation layers mimicking real building insulation practices. The experiment aimed to control and monitor the internal temperatures of these houses by alternately placing them in a 50°C oven and a 0°C refrigerator, each for periods of 10 mins. This temperature regimen was chosen to replicate more severe environmental conditions, thereby creating a

significant temperature differential to assess the effectiveness of the PCM films under extreme conditions.

In the design of the simulated houses, PCM films were strategically installed on the interiors of the roofs and walls, but deliberately excluded from the floors. This decision was based on practical considerations in real-world applications where film-type materials are typically unsuitable for flooring due to potential wear and tear from traffics and other mechanical impacts. Temperature monitoring within the houses was conducted using two calibrated electronic thermometers to minimize experimental error. Calibration was performed prior to the experimental runs to ensure accuracy, and the procedure was repeated three times to confirm the reliability and repeatability of the results. The data collected from these thermometers were analyzed using professional software provided by the thermometer manufacturer, enabling precise and systematic evaluation of the thermal performance of the PCM films within the simulated house environment. This methodological approach provides a scientifically robust framework for understanding the potential of PCM films in enhancing thermal regulation in green building contexts.

5.1.2 Experimental design of human skin application

To assess the effectiveness of flexible phase change films when applied to human skin, a meticulous experimental design was implemented. Initially, the film was tailored into 3 x 3 cm squares using precision cutting tools to ensure compatibility with the dimensions of the dorsal aspect of the human hand. Subsequently, the film was securely adhered to the designated area on the back of the hand, as depicted in Figure 24. The experimental protocol involved simulating exposure to a cooler environment by applying a low-temperature water bag directly over the film on the hand. This setup aimed to replicate the skin's contact with colder conditions. Equilibrium at this lower temperature was confirmed using an infrared thermal imager, ensuring that both the skin and the phase change film were uniformly cooled. Following this stabilization phase, the water bag was removed, allowing the temperature of the hand and the film to gradually return to ambient room conditions. This process simulated a natural warming environment, mimicking the typical temperature variations one might experience. Throughout this procedure, temperature variations were continuously monitored and recorded with an infrared thermal imager. The imager was securely mounted on a tripod set at a 50 cm distance from the subject to minimize any disruptions caused by physical movements or environmental factors. To uphold the scientific rigor and ensure the reproducibility of the results, the experiment was conducted three times, each yielding comparable outcomes. This repeated testing underscores the reliability and consistency of the experimental results, confirming the phase change film’s potential for practical application on human skin in varying thermal environments.

5.1.3 Experimental design of portable electronic equipment application

To evaluate the suitability of flexible phase change films for thermal management in electronic devices, a structured experimental design was formulated and executed. The initial phase involved precisely cutting the phase change film into 3 x 9 cm sections using scissors,

dimensions specifically chosen to cover the significant heating areas of a typical portable cell phone. This customization was crucial given the non-uniform temperature distribution across mobile devices due to varying internal component layouts and disparate heating efficiencies. The target area for the application of the film was determined through preliminary infrared imaging of the mobile phone, which identified the region beneath the camera as the primary heat generation zone. Subsequently, the film was meticulously affixed to this area on the back of the phone, as documented in Figure 25.

Prior to initiating the temperature elevation procedures, the baseline temperature of both the mobile phone's back and the phase change film was ascertained using an infrared thermal imager to ensure uniform starting conditions. The experimental conditions were then manipulated by simultaneously running intensive software applications and charging the device, activities known to induce significant thermal output.

Throughout the duration of the experiment, a fixed infrared thermal imager, stationed on a tripod approximately 50 cm away from the subject, continuously monitored and recorded the temporal temperature changes. This setup minimized any potential disturbances from external vibrations or other environmental variables. To uphold the scientific integrity and confirm the repeatability of the findings, this experiment was conducted three times, each instance producing comparable results. This rigorous testing protocol confirms the effectiveness of phase change films in managing the thermal output of electronic devices under operational stresses, demonstrating their potential to enhance device performance and longevity by providing heat management.

5.2 Simulation house application

Fig. 23a provides a clear demonstration of the benefits of incorporating PCMs in building design, particularly emphasizing their ability to stabilize indoor temperatures effectively over time. This graph compares temperature fluctuations within a simulated house environment over a 120-minute period, contrasting scenarios with and without PCM integration. The setup that includes PCM maintains a consistent temperature range between 20°C and 29°C, showcasing its capability to moderate temperature extremes efficiently. This contrasts sharply with the environment lacking PCM, where temperatures swing broadly between 10°C and 35°C. Such stabilization is crucial not only for enhancing occupant comfort but also for reducing the energy demands typically associated with mechanical heating and cooling systems.

Importantly, the data from Fig. 23a also highlights the long-term viability and reusability of PCMs in practical applications. The ability of PCM to repeatedly absorb and release heat during cyclic temperature changes without significant degradation shows its potential for prolonged use. This repeated cycle of thermal absorption and release underlines PCM's role in sustainable building practices, where it can be employed to continually adjust and regulate the indoor climate based on external thermal conditions. This capacity for long-term, repetitive use without loss of efficiency demonstrates PCM's suitability for inclusion in green building designs aimed at achieving long-term energy savings. By ensuring a consistent indoor environment with reduced energy

expenditure on heating and cooling, PCMs not only support current sustainability goals but also contribute to the resilience and adaptability of modern construction methods, enhancing the overall lifecycle of building environments.

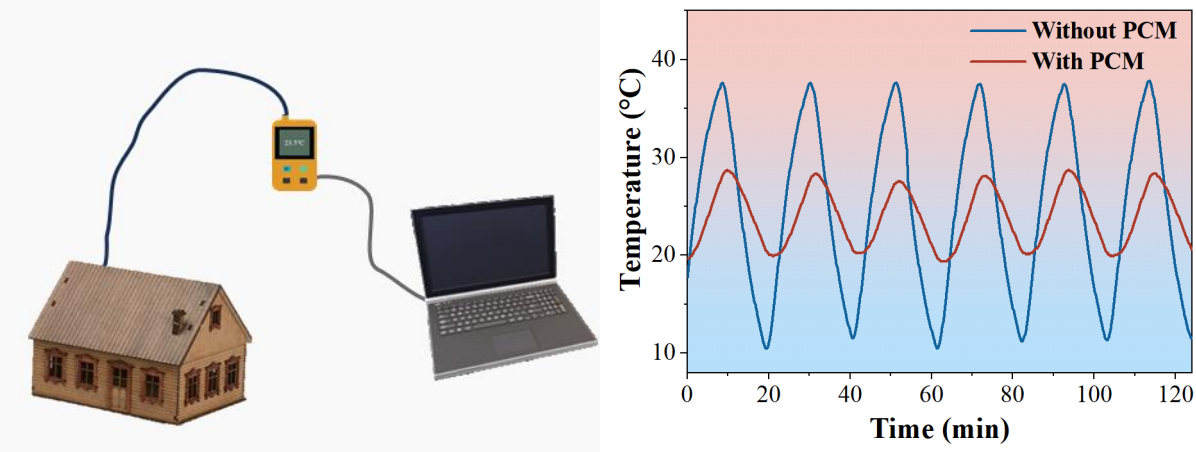

Figure 23. (a) Illustration image for the simulation house application. (b) Temperature curve of the model house application.

5.3 human skin application

Fig. 24 presents a series of infrared images documenting the thermal response of a PCM film applied to human skin over 300 seconds. These images provide a visual comparison of temperature changes between the PCM-covered skin and the adjacent uncovered skin, highlighting the film's thermal management capabilities. The infrared images from Fig. 24 show a clear distinction in color between the areas covered by the PCM film and the exposed skin. Initially, at 60 seconds, the temperature over the film is recorded at 19.1°C, and as time progresses—120s at 21.5°C, 180s at 22.3°C, 240s at 24.2°C, and 300s at 25.7°C—the film consistently exhibits a darker color compared to the surrounding skin. This color difference indicates that the temperature of the PCM-covered area remains consistently lower than that of the uncovered skin.

The consistent lower temperature of the PCM film as compared to the adjacent skin suggests effective heat absorption and thermal regulation by the PCM. The darker coloration of the film in infrared imaging is indicative of its lower temperature, providing visual evidence of the film’s phase change activity. As the PCM absorbs heat from the skin and the surrounding environment, it undergoes a phase change, which effectively dissipates the absorbed heat, thereby moderating the temperature rise. The thermal behavior captured in Fig. 24 confirms the efficacy of PCM films in maintaining cooler temperatures compared to uncovered skin, highlighting their potential in applications requiring precise thermal control. The PCM film's ability to consistently maintain cooler temperatures under a heat load demonstrates its dual functionality in thermal

energy management. By absorbing excess heat to prevent overheating and releasing stored heat to avoid overcooling, the PCM ensures an optimal thermal comfort zone. This bidirectional thermal regulation makes PCM films highly suitable for incorporation into wearable technologies and medical devices, where maintaining a stable skin temperature is crucial for user comfort and safety. The demonstrated efficiency of PCM films in managing thermal fluctuations underscores their potential as a versatile solution for dynamic thermal management across various applications.

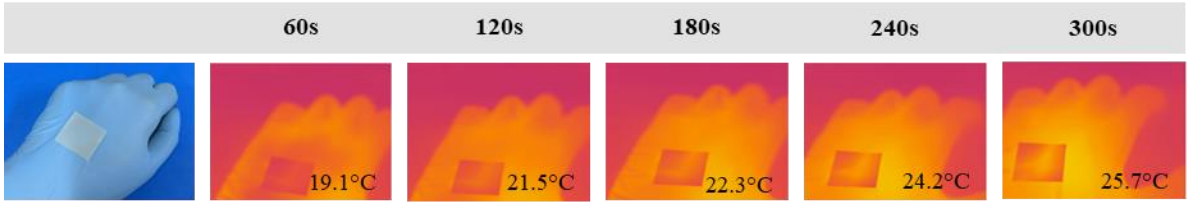

Figure 24. Digital images and the infrared images for the human skin application.

5.4 portable electronic equipment application

Fig. 25 illustrates a series of infrared images capturing the temperature progression of a PCM film applied to a portable electronic device (specifically, a mobile phone) over a period of 300 seconds. This experiment was designed to evaluate the effectiveness of PCM films in managing the thermal output of electronic devices during operation. The sequence begins at 60 seconds with the PCM film showing a temperature of 26.8°C, and over time, it incrementally rises to 31.8°C by 300 seconds. Notably, throughout the experiment, the areas covered by the PCM film are visually distinct in the infrared images, displaying darker colors compared to the brighter, warmer colors of the uncovered areas of the phone. This contrast is significant at each time interval, highlighting the film's impact on the surface temperature.

The darker color of the PCM-covered areas compared to the brighter hues of the phone's exposed surfaces indicates that the PCM film is effectively managing the device's heat output. The film absorbs and dissipates thermal energy, moderating the temperature rise even as the device undergoes normal operational stress, such as running software or charging, which typically generate substantial heat. This temperature regulation is critical not only for user comfort but also for maintaining the device's operational integrity and prolonging its lifespan. The results from Fig. 25 demonstrate that PCM films are highly effective in controlling and stabilizing temperatures in portable electronic devices. By visually comparing the cooler, darker colors of the PCM-treated areas with the warmer, brighter colors of untreated sections, it is evident that the PCM film plays a significant role in heat management. This ability to moderate temperature fluctuations underlines

the potential of PCM films to enhance the performance and durability of consumer electronics, making them a practical solution for improving device safety and user experience.

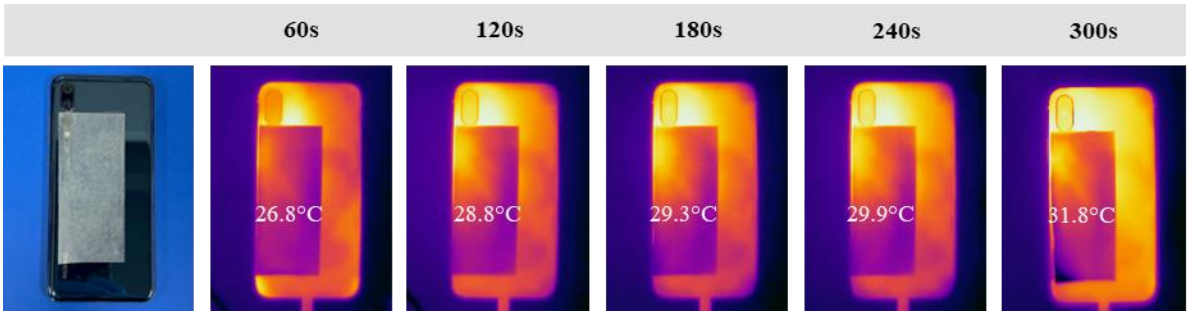

Figure 25. Digital and infrared images for the portable electronic equipment application.

5.5 Conclusions

This part examined the practical uses of PCM films, proving their adaptability and effectiveness in a variety of industries including as energy storage, building management, textiles, and electronics. In the realm of green building, as shown in our simulation house application experiment, PCM films have proven to effectively stabilize indoor temperatures, reducing the energy demands typically associated with mechanical heating and cooling systems. This capability not only enhances occupant comfort but also contributes to long-term energy savings and sustainability by continuously adjusting and regulating the indoor climate based on external thermal conditions. For wearable technology applications, our experiments on human skin have validated PCM films' ability to maintain comfortable skin temperatures, effectively absorbing and dissipating heat to prevent discomfort or thermal stress. This attribute is particularly valuable in personal thermal comfortable applications where maintaining specific thermal conditions is crucial for comfort and safety. In the electronics sector, our findings from the portable electronic equipment application illustrate that PCM films can significantly improve thermal management in devices such as mobile phones. By controlling and stabilizing temperature fluctuations, these films enhance device performance and longevity, preventing overheating and the potential damage it can cause. Overall, the practical applications of PCM films as demonstrated through these case studies highlight their potential to revolutionize thermal regulation technologies across multiple industries. By bridging the gap between theoretical research and practical implementation, PCM films stand out as a transformative solution, offering substantial impacts and commercial viability in addressing complex thermal management challenges.

6. Conclusions and innovations

6.1 Conclusions

This thesis has delineated the integration of advanced materials such as hectorite and GNP into phase change material films and demonstrated their enhanced capabilities through various experimental designs, each focusing on distinct practical applications. The investigations span multiple sectors, including building management, electronics, and personal care, emphasizing the versatility and essential role of PCM films in modern thermal management technologies.

The first part of the study explored the role of hectorite in reinforcing the mechanical properties and fire retardancy of PCM films comprising PEG and CNF. The inclusion of hectorite significantly increased the structural integrity and thermal stability of the films. For instance, PEG/CNF films without hectorite showed a tensile strength of 9.56 MPa and a fracture strain of 3.92%. In contrast, films incorporated with hectorite exhibited enhanced tensile strength of 16.84 MPa and a modified fracture strain of 3.27%. These improvements make the PCM films more durable and suitable for applications where mechanical robustness and fire safety are critical, such as in wearable devices, flexible electronics, and sustainable building materials.

The second part of the thesis focused on the integration of GNP, which significantly augmented the photothermal and thermal regulation properties of the PCM films. The films with GNP displayed markedly improved heat absorption and dissipation rates, characteristics beneficial for applications requiring rapid thermal response, such as in aerospace, automotive, and advanced electronic cooling systems. Enhanced PCM films with GNP demonstrated quicker and more pronounced temperature regulation capabilities, highlighting the critical role of GNP in advancing PCM film technology for high-performance applications.

Finally, the practical applications of PCM films were extensively explored, demonstrating their effectiveness in real-world settings. The films proved to be extraordinarily versatile, capable of efficiently regulating temperature in diverse environments. In green building applications, PCM films effectively stabilized indoor temperatures, significantly reducing reliance on conventional heating and cooling systems and thereby enhancing energy efficiency and occupant comfort. In wearable and medical technologies, the films maintained cooler skin temperatures, mitigating thermal discomfort. Furthermore, in the electronics sector, PCM films improved the thermal management of devices, preventing overheating and extending device longevity.

Overall, this thesis presents compelling evidence that PCM films, especially those enhanced with hectorite and GNP, offer substantial benefits across a broad range of applications. By improving mechanical strength, fire retardancy, and thermal management capabilities, these enhanced films meet the critical demands of modern technologies. The integration of such innovative materials into PCM films not only bridges the gap between theoretical research and

practical application but also paves the way for revolutionary advances in thermal regulation technology. The findings from this research underscore the potential of PCM films to significantly impact multiple industries, promising substantial commercial viability and contributing to the advancement of sustainable and efficient thermal management solutions.

6.2 Innovations

The development of composite flexible phase change films represents a significant innovation in addressing the inherent rigidity of traditional phase change materials. This research advances the field by enhancing the films' mechanical strength, fire resistance, thermal conductivity, and photothermal properties. By integrating mineral materials and graphene to create a robust support structure within the films, this work introduces a novel design approach that not only maintains flexibility but also adds multifunctional capabilities to the phase change films. This innovative strategy enhances the functional performance of PCMs and expands their application range, thereby facilitating the high-value utilization of mineral resources. Such advancements open new avenues for employing mineral materials across various industries, significantly boosting their practical and economic value.

This thesis introduces a transformative innovation by experimentally validating the practical applications of PCM films across multiple real-world settings. Demonstrating the films' ability to effectively manage indoor temperatures in buildings, regulate skin temperatures in wearable technology, and prevent overheating in electronics, the research underscores the versatility and utility of PCM films in practical applications. A significant breakthrough of this work is bridging the gap between theoretical research and practical implementation. By converting laboratory enhancements into viable, real-world solutions, the thesis turns conceptual advancements into applicable technologies that significantly improve energy efficiency, safety, and device longevity across various industries. This alignment of theoretical innovation with practical utility marks a pivotal advancement in materials science and thermal management, setting new benchmarks for the development and application of PCM films

6.3 Future expectations

The future development on PCM films could focus on several promising areas. One key direction is the exploration of advanced material combinations. Future studies could investigate the integration of innovative materials such as nanotechnology, bio-based components, or hybrid composites to enhance the thermal and mechanical properties of PCM films, potentially introducing functionalities like improved environmental sustainability or self-healing capabilities.

Another vital area for advancement lies in scaling and optimizing manufacturing processes. There is a significant opportunity to develop continuous production techniques that ensure the consistent quality and performance of PCM films, making them suitable for large-scale industrial applications. This could help reduce production costs and increase the accessibility of PCM technologies across various sectors.

Additionally, expanding the application domains of PCM films is crucial. While current applications include building management, wearable technology, and electronics, future research could extend these applications to sectors such as automotive and aerospace, where efficient thermal management is critically needed.

Acknowledgement

I am deeply grateful to my advisors, Dr. Shaoxian Song, Dr. Bernardo José Luis Arauz Lara, and Dr. Hao Yi, for their invaluable guidance, support, and mentorship throughout my research journey. Each has contributed uniquely to my academic development and the success of this thesis. Dr. Song's insightful feedback, Dr. Arauz Lara's expert advice, and Dr. Yi's rigorous analytical approaches have profoundly shaped my work and scholarly growth. I also extend my gratitude to all my peers in Dr. Song's lab, whose assistance and camaraderie have greatly enriched my research experience. Their support has been indispensable in navigating the challenges of my thesis work.

On a personal note, my heartfelt thanks go to my parents and family, whose constant encouragement and belief in my abilities have sustained me throughout this process. I must also mention my cat Ryan, whose companionship has brought me immeasurable comfort and joy during this intense academic pursuit. My last tribute is to those who know I am not perfect but still love me. This thesis would not have been possible without the collective support and encouragement of everyone mentioned here. I am truly thankful for their contributions to my journey. May our life stir up ripples in the tranquil spring.

Keqiao (Chelsea) Gao

References

[1] F. Liu *et al.*, “Low Cost, Robust, Environmentally Friendly Geopolymer–Mesoporous Carbon Composites for Efficient Solar Powered Steam Generation,” *Adv Funct Mater*, vol. 28, no. 47, 2018, doi: 10.1002/ADFM.201803266.

[2] “Nanocellulose-based composite phase change materials for thermal energy storage: status and challenges - Energy & Environmental Science (RSC Publishing).” [Online]. Available: https://pubs.rsc.org/en/content/articlelanding/2023/EE/D2EE04063H

[3] Q. Zhang *et al.*, “Biomass Homogeneity Reinforced Carbon Aerogels Derived Functional Phase-Change Materials for Solar–Thermal Energy Conversion and Storage,” *Energy and Environmental Materials*, vol. 6, no. 1, 2023, doi: 10.1002/eem2.12264.

[4] Z. Shen, M. Qin, F. Xiong, R. Zou, and J. Zhang, “Nanocellulose-based composite phase change materials for thermal energy storage: status and challenges,” *Energy and Environmental Science*, vol. 16, no. 3. Royal Society of Chemistry, pp. 830–861, 2023. doi: 10.1039/d2ee04063h.

[5] A. Muthumeenal, S. Sundar Pethaiah, and A. Nagendran, “Biopolymer Composites in Fuel Cells,” *Biopolymer Composites in Electronics*, pp. 185–217, 2017, doi: 10.1016/B978-0-12-809261-3.00006-1.

[6] C. Withagen, “Pollution and exhaustibility of fossil fuels,” *Resour Energy Econ*, vol. 16, no. 3, 1994, doi: 10.1016/0928-7655(94)90007-8.

[7] P. Tao *et al.*, “Solar-driven interfacial evaporation,” *Nat Energy*, vol. 3, no. 12, pp. 1031–1041, 2018, doi: 10.1038/S41560-018-0260-7.

[8] H. Ren *et al.*, “Hierarchical Graphene Foam for Efficient Omnidirectional Solar–Thermal Energy Conversion,” *Advanced Materials*, vol. 29, no. 38, 2017, doi: 10.1002/ADMA.201702590.

[9] H. Yi *et al.*, “A novel core-shell structural montmorillonite nanosheets/stearic acid composite PCM for great promotion of thermal energy storage properties,” *Solar Energy Materials and Solar Cells*, vol. 192, pp. 57–64, 2019, doi: 10.1016/j.solmat.2018.12.015.

[10] H. Yi, Z. Ai, Y. Zhao, X. Zhang, and S. Song, “Design of 3D-network montmorillonite nanosheet/stearic acid shape-stabilized phase change materials for solar energy storage,” *Solar Energy Materials and Solar Cells*, vol. 204, 2020, doi: 10.1016/j.solmat.2019.110233.

[11] H. Yi, L. Xia, and S. Song, “Three-dimensional montmorillonite/Ag nanowire aerogel supported stearic acid as composite phase change materials for superior solar-thermal

energy harvesting and storage," *Compos Sci Technol*, vol. 217, 2022, doi: 10.1016/j.compscitech.2021.109121.

[12] I. Sarbu and C. Sebarchievici, "A comprehensive review of thermal energy storage," *Sustainability (Switzerland)*, vol. 10, no. 1, 2018, doi: 10.3390/SU10010191.

[13] C. Suresh and R. P. Saini, "Performance comparison of sensible and latent heat-based thermal storage system during discharging–an experimental study," *Experimental Heat Transfer*, vol. 35, no. 1, pp. 45–61, 2022, doi: 10.1080/08916152.2020.1817178.

[14] N. Ahmed, K. E. Elfeky, L. Lu, and Q. W. Wang, "Thermal and economic evaluation of thermocline combined sensible-latent heat thermal energy storage system for medium temperature applications," *Energy Convers Manag*, vol. 189, pp. 14–23, 2019, doi: 10.1016/J.ENCONMAN.2019.03.040.

[15] H. Zhang, J. Baeyens, G. Cáceres, J. Degrève, and Y. Lv, "Thermal energy storage: Recent developments and practical aspects," *Prog Energy Combust Sci*, vol. 53, pp. 1–40, Mar. 2016, doi: 10.1016/J.PECS.2015.10.003.

[16] J. Sunku Prasad, P. Muthukumar, F. Desai, D. N. Basu, and M. M. Rahman, "A critical review of high-temperature reversible thermochemical energy storage systems," *Appl Energy*, vol. 254, 2019, doi: 10.1016/J.APENERGY.2019.113733.

[17] A. Kumar and A. Kumar, "Heat transfer analysis in thermal energy storage—A comprehensive review-based latent heat storage system," *Energy Storage*, 2022, doi: 10.1002/EST2.434.

[18] A. Abhat, "Low temperature latent heat thermal energy storage: Heat storage materials," *Solar Energy*, vol. 30, no. 4, pp. 313–332, 1983, doi: 10.1016/0038-092X(83)90186-X.

[19] D. A. Neeper, "Thermal dynamics of wallboard with latent heat storage," *Solar Energy*, vol. 68, no. 5, pp. 393–403, 2000, doi: 10.1016/S0038-092X(00)00012-8.

[20] J. Zhu, Q. An, Q. Guo, H. Yi, L. Xia, and S. Song, "Mechanically strong hectorite aerogel encapsulated octadecane as shape-stabilized phase change materials for thermal energy storage and management," *Appl Clay Sci*, vol. 223, 2022, doi: 10.1016/j.clay.2022.106511.

[21] W. Aftab, A. Usman, J. Shi, K. Yuan, M. Qin, and R. Zou, "Phase change material-integrated latent heat storage systems for sustainable energy solutions," *Energy and Environmental Science*, vol. 14, no. 8. Royal Society of Chemistry, pp. 4268–4291, 2021. doi: 10.1039/d1ee00527h.

[22] Y. Dutil, D. R. Rousse, N. Ben Salah, S. Lassue, and L. Zalewski, "A review on phase-change materials: Mathematical modeling and simulations," *Renewable and Sustainable Energy Reviews*, vol. 15, no. 1, pp. 112–130, 2011, doi: 10.1016/j.rser.2010.06.011.

[23] R. Guo *et al.*, “Phase-change materials for intelligent temperature regulation,” *Materials Today Energy*, vol. 23. Elsevier Ltd, 2022. doi: 10.1016/j.mtener.2021.100888.

[24] W. Dai *et al.*, “A Paper-Like Inorganic Thermal Interface Material Composed of Hierarchically Structured Graphene/Silicon Carbide Nanorods,” *ACS Nano*, vol. 13, no. 2, pp. 1547–1554, 2019, doi: 10.1021/ACSNANO.8B07337.

[25] N. Xie, Z. Huang, Z. Luo, X. Gao, Y. Fang, and Z. Zhang, “Inorganic salt hydrate for thermal energy storage,” *Applied Sciences (Switzerland)*, vol. 7, no. 12, 2017, doi: 10.3390/APP7121317.

[26] P. Karimineghlani, E. Emmons, M. J. Green, P. Shamberger, and S. A. Sukhishvili, “A temperature-responsive poly(vinyl alcohol) gel for controlling fluidity of an inorganic phase change material,” *J Mater Chem A Mater*, vol. 5, no. 24, pp. 12474–12482, 2017, doi: 10.1039/C7TA02897K.

[27] Y. Wang, B. Tang, and S. Zhang, “Organic, cross-linking, and shape-stabilized solar thermal energy storage materials: A reversible phase transition driven by broadband visible light,” *Appl Energy*, vol. 113, pp. 59–66, 2014, doi: 10.1016/j.apenergy.2013.07.007.

[28] N. Sarier and E. Onder, “Organic phase change materials and their textile applications: An overview,” *Thermochim Acta*, vol. 540, pp. 7–60, 2012, doi: 10.1016/J.TCA.2012.04.013.

[29] M. A. Gerkman and G. G. D. Han, “Toward Controlled Thermal Energy Storage and Release in Organic Phase Change Materials.”

[30] L. Wang and D. Meng, “Fatty acid eutectic/polymethyl methacrylate composite as form-stable phase change material for thermal energy storage,” *Appl Energy*, vol. 87, no. 8, pp. 2660–2665, 2010, doi: 10.1016/J.APENERGY.2010.01.010.

[31] L. Cao, Y. Tang, and G. Fang, “Preparation and properties of shape-stabilized phase change materials based on fatty acid eutectics and cellulose composites for thermal energy storage,” *Energy*, vol. 80, pp. 98–103, 2015, doi: 10.1016/j.energy.2014.11.046.

[32] P. Singh, R. K. Sharma, A. K. Ansu, R. Goyal, A. Sarı, and V. V Tyagi, “A comprehensive review on development of eutectic organic phase change materials and their composites for low and medium range thermal energy storage applications,” *Solar Energy Materials and Solar Cells*, vol. 223, 2021, doi: 10.1016/J.SOLMAT.2020.110955.

[33] S. Phadungphatthanakoon, S. Poompradub, and S. P. Wanichwecharungruang, “Increasing the thermal storage capacity of a phase change material by encapsulation: Preparation and application in natural rubber,” *ACS Appl Mater Interfaces*, vol. 3, no. 9, pp. 3691–3696, 2011, doi: 10.1021/AM200870E.

[34] Y. Huang, A. Stonehouse, and C. Abeykoon, “Encapsulation methods for phase change materials – A critical review,” *Int J Heat Mass Transf*, vol. 200, p. 123458, 2023, doi: 10.1016/J.IJHEATMASSTRANSFER.2022.123458.

[35] T. Khadiran, M. Z. Hussein, Z. Zainal, and R. Rusli, “Encapsulation techniques for organic phase change materials as thermal energy storage medium: A review,” *Solar Energy Materials and Solar Cells*, vol. 143, pp. 78–98, 2015, doi: 10.1016/J.SOLMAT.2015.06.039.

[36] G. H. Feng, D. Liang, K. L. Huang, and Y. Wang, “Thermal performance difference of phase change energy storage units based on tubular macro-encapsulation,” *Sustain Cities Soc*, vol. 50, 2019, doi: 10.1016/j.scs.2019.101662.

[37] K. Liu, Z. F. Yuan, H. X. Zhao, C. H. Shi, and F. Zhao, “Properties and applications of shape-stabilized phase change energy storage materials based on porous material support—A review,” *Materials Today Sustainability*, vol. 21, 2023, doi: 10.1016/j.mtsust.2023.100336.

[38] X. Huang *et al.*, “Shape-stabilized phase change materials based on porous supports for thermal energy storage applications,” *Chemical Engineering Journal*, vol. 356, pp. 641–661, 2019, doi: 10.1016/j.cej.2018.09.013.

[39] T. Jiang *et al.*, “Biomass-derived porous carbons support in phase change materials for building energy efficiency: a review,” *Materials Today Energy*, vol. 23. Elsevier Ltd, 2022. doi: 10.1016/j.mtener.2021.100905.

[40] M. Jiang, X. Song, G. Ye, and J. Xu, “Preparation of PVA/paraffin thermal regulating fiber by in situ microencapsulation,” *Compos Sci Technol*, vol. 68, no. 10–11, pp. 2231–2237, 2008, doi: 10.1016/j.compscitech.2008.04.004.

[41] X. Huo *et al.*, “Chitosan composite microencapsulated comb-like polymeric phase change material via coacervation microencapsulation,” *Carbohydr Polym*, vol. 200, pp. 602–610, 2018, doi: 10.1016/j.carbpol.2018.08.003.

[42] X. Shi, M. R. Yazdani, R. Ajdary, and O. J. Rojas, “Leakage-proof microencapsulation of phase change materials by emulsification with acetylated cellulose nanofibrils,” *Carbohydr Polym*, vol. 254, 2021, doi: 10.1016/j.carbpol.2020.117279.

[43] A. Jamekhorshid, S. M. Sadrameli, and M. Farid, “A review of microencapsulation methods of phase change materials (PCMs) as a thermal energy storage (TES) medium,” *Renewable and Sustainable Energy Reviews*, vol. 31, pp. 531–542, 2014, doi: 10.1016/J.RSER.2013.12.033.

[44] D. G. Prajapati and B. Kandasubramanian, “A Review on Polymeric-Based Phase Change Material for Thermo-Regulating Fabric Application,” *Polymer Reviews*, vol. 60, no. 3, pp. 389–419, 2020, doi: 10.1080/15583724.2019.1677709.

[45] S. Fujisawa, Y. Takasaki, and T. Saito, “Structure of Polymer-Grafted Nanocellulose in the Colloidal Dispersion System,” *Nano Lett*, vol. 23, no. 3, pp. 880–886, 2023, doi: 10.1021/acs.nanolett.2c04138.

[46] C. P. Feng *et al.*, “Recent advances in polymer-based thermal interface materials for thermal management: A mini-review,” *Composites Communications*, vol. 22, 2020, doi: 10.1016/J.COCO.2020.100528.

[47] G. Z. Yin, J. Hobson, Y. Duan, and D. Y. Wang, “Polyrotaxane: New generation of sustainable, ultra-flexible, form-stable and smart phase change materials,” *Energy Storage Mater*, vol. 40, pp. 347–357, 2021, doi: 10.1016/j.ensm.2021.05.023.

[48] Y. Huan *et al.*, “Highly flexible, healable and degradable polyurethane phase change materials with exceptional mechanical properties for thermal regulation,” *Chemical Engineering Journal*, vol. 468, 2023, doi: 10.1016/j.cej.2023.143742.

[49] J. Shi, M. Qin, W. Aftab, and R. Zou, “Flexible phase change materials for thermal energy storage,” *Energy Storage Materials*, vol. 41. Elsevier B.V., pp. 321–342, 2021. doi: 10.1016/j.ensm.2021.05.048.

[50] C. Wang, K. Xia, H. Wang, X. Liang, Z. Yin, and Y. Zhang, “Advanced Carbon for Flexible and Wearable Electronics,” *Advanced Materials*, vol. 31, no. 9, 2019, doi: 10.1002/ADMA.201801072.

[51] X. Zhao, D. Zou, and S. Wang, “Flexible phase change materials: Preparation, properties and application,” *Chemical Engineering Journal*, vol. 431, p. 134231, 2022, doi: 10.1016/J.CEJ.2021.134231.

[52] L. Zhang, X. L. Shi, Y. L. Yang, and Z. G. Chen, “Flexible thermoelectric materials and devices: From materials to applications,” *Materials Today*, vol. 46. Elsevier B.V., pp. 62–108, 2021. doi: 10.1016/j.mattod.2021.02.016.

[53] Z. Fan, Y. Zhang, L. Pan, J. Ouyang, and Q. Zhang, “Recent developments in flexible thermoelectrics: From materials to devices,” *Renewable and Sustainable Energy Reviews*, vol. 137, 2021, doi: 10.1016/J.RSER.2020.110448.

[54] Y. Kou *et al.*, “An intrinsically flexible phase change film for wearable thermal managements,” *Energy Storage Mater*, vol. 34, pp. 508–514, 2021, doi: 10.1016/j.ensm.2020.10.014.

[55] P. Cheng, Z. Tang, Y. Gao, P. Liu, C. Liu, and X. Chen, “Flexible engineering of advanced phase change materials,” *iScience*, vol. 25, no. 5, May 2022, doi: 10.1016/J.ISCI.2022.104226.

[56] Y. Zhang, B. Tang, L. Wang, R. Lu, D. Zhao, and S. Zhang, “Novel hybrid form-stable polyether phase change materials with good fire resistance,” *Energy Storage Mater*, vol. 6, pp. 46–52, 2017, doi: 10.1016/j.ensm.2016.10.001.

[57] Y. Jiang, P. Yan, Y. Wang, C. Zhou, and J. Lei, “Form-stable phase change materials with enhanced thermal stability and fire resistance via the incorporation of phosphorus and silicon,” *Mater Des*, vol. 160, pp. 763–771, 2018, doi: 10.1016/j.matdes.2018.10.020.

[58] J. Yang *et al.*, “Exploring Next-Generation Functional Organic Phase Change Composites,” *Advanced Functional Materials*, vol. 32, no. 28. John Wiley and Sons Inc, 2022. doi: 10.1002/adfm.202200792.

[59] R. D. McGillicuddy, S. Thapa, M. B. Wenny, M. I. Gonzalez, and J. A. Mason, “Metal-organic phase-change materials for thermal energy storage,” *J Am Chem Soc*, vol. 142, no. 45, pp. 19170–19180, 2020, doi: 10.1021/jacs.0c08777.

[60] M. M. Kenisarin, “Thermophysical properties of some organic phase change materials for latent heat storage. A review,” *Solar Energy*, vol. 107, pp. 553–575, 2014, doi: 10.1016/J.SOLENER.2014.05.001.

[61] Q. Sun, H. Zhang, J. Xue, X. Yu, Y. Yuan, and X. Cao, “Flexible phase change materials for thermal storage and temperature control,” *Chemical Engineering Journal*, vol. 353, pp. 920–929, 2018, doi: 10.1016/j.cej.2018.07.185.

[62] S. Gong *et al.*, “High Thermal Conductivity and Mechanical Strength Phase Change Composite with Double Supporting Skeletons for Industrial Waste Heat Recovery,” *ACS Appl Mater Interfaces*, vol. 13, no. 39, pp. 47174–47184, 2021, doi: 10.1021/ACSAMI.1C15670.

[63] X. Lu, H. Yu, L. Zhang, Y. Zheng, L. Xu, and Y. Zhao, “Flexible Ethylene Propylene Diene Monomer/Paraffin Wax Vulcanizate with Simultaneously Increased Mechanical Strength, Thermal-Energy Storage, and Shape-Memory Behavior,” *Energy and Fuels*, vol. 34, no. 7, pp. 9020–9029, 2020, doi: 10.1021/ACS.ENERGYFUELS.0C01800.

[64] J. Chen *et al.*, “Photothermal Membrane of CuS/Polyacrylamide-Carboxymethyl Cellulose for Solar Evaporation,” *ACS Appl Polym Mater*, vol. 3, no. 5, pp. 2402–2410, 2021, doi: 10.1021/ACSAPM.0C01422.

[65] S. Hou, M. Wang, S. Guo, and M. Su, “Photothermally Driven Refreshable Microactuators Based on Graphene Oxide Doped Paraffin,” *ACS Appl Mater Interfaces*, vol. 9, no. 31, pp. 26476–26482, 2017, doi: 10.1021/ACSAMI.7B08728.

[66] Z. Yang *et al.*, “Thermally conductive, dielectric PCM-boron nitride nanosheet composites for efficient electronic system thermal management,” *Nanoscale*, vol. 8, no. 46, pp. 19326–19333, 2016, doi: 10.1039/C6NR07357C.

[67] C. P. Feng *et al.*, “Emerging Flexible Thermally Conductive Films: Mechanism, Fabrication, Application,” *Nanomicro Lett*, vol. 14, no. 1, 2022, doi: 10.1007/S40820-022-00868-8.

[68] A. Li *et al.*, “Hierarchical 3D Reduced Graphene Porous-Carbon-Based PCMs for Superior Thermal Energy Storage Performance,” *ACS Appl Mater Interfaces*, vol. 10, no. 38, pp. 32093–32101, 2018, doi: 10.1021/ACSAMI.8B09541.

[69] S. Li *et al.*, “Hierarchical porous aero-cryogels for wind energy enhanced solar vapor generation,” *Cellulose*, vol. 29, no. 2, pp. 953–966, 2022, doi: 10.1007/s10570-021-04335-2.

[70] Y. Li, X. Huang, J. Lv, F. Wang, S. Jiang, and G. Wang, “Enzymolysis-treated wood-derived hierarchical porous carbon for fluorescence-functionalized phase change materials,” *Compos B Eng*, vol. 234, 2022, doi: 10.1016/j.compositesb.2022.109735.

[71] K. Zhang, P. Tao, Y. Zhang, X. Liao, and S. Nie, “Highly thermal conductivity of CNF/AlN hybrid films for thermal management of flexible energy storage devices,” *Carbohydr Polym*, vol. 213, pp. 228–235, 2019, doi: 10.1016/J.CARBPOL.2019.02.087.

[72] S. B. Entürk, D. Kahraman, C. Alkan, and I. Göke, “Biodegradable PEG/cellulose, PEG/agarose and PEG/chitosan blends as shape stabilized phase change materials for latent heat energy storage,” *Carbohydr Polym*, vol. 84, no. 1, pp. 141–144, 2011, doi: 10.1016/j.carbpol.2010.11.015.

[73] C. Zhu *et al.*, “Constructing heat conduction path and flexible support skeleton for PEG-based phase change composites through salt template method,” *Compos Sci Technol*, vol. 226, 2022, doi: 10.1016/j.compscitech.2022.109532.

[74] R. Scaffaro *et al.*, “Synthesis and self-assembly of a PEGylated-graphene aerogel,” *Compos Sci Technol*, vol. 128, pp. 193–200, 2016, doi: 10.1016/j.compscitech.2016.03.030.

[75] X. Min *et al.*, “Enhanced thermal properties of novel shape-stabilized PEG composite phase change materials with radial mesoporous silica sphere for thermal energy storage,” *Sci Rep*, vol. 5, 2015, doi: 10.1038/SREP12964.

[76] A. Chakrabarty and Y. Teramoto, “Efficient Phase-Change Polymer Composite Film from Emulsion Gels Stabilized by Cellulose Nanofiber-Based Amphiphiles,” *ACS Appl Polym Mater*, vol. 3, no. 11, pp. 5441–5451, 2021, doi: 10.1021/acsapm.1c00769.

[77] B. Fan, S. Chen, Q. Yao, Q. Sun, and C. Jin, “Fabrication of cellulose nanofiber/AlOOH aerogel for flame retardant and thermal insulation,” *Materials*, vol. 10, no. 3, 2017, doi: 10.3390/ma10030311.

[78] G. E. Christidis *et al.*, “The nature of laponite: Pure hectorite or a mixture of different trioctahedral phases?,” *Minerals*, vol. 8, no. 8, 2018, doi: 10.3390/min8080314.

[79] D. Tong, K. Fang, H. Yang, J. Wang, C. Zhou, and W. Yu, “Efficient removal of copper ions using a hydrogel bead triggered by the cationic hectorite clay and anionic sodium alginate,” *Environmental Science and Pollution Research*, vol. 26, no. 16, pp. 16482–16492, Jun. 2019, doi: 10.1007/S11356-019-04895-8.

[80] Y. Liu, H. Liu, and H. Qi, “High efficiency electro- and photo-thermal conversion cellulose nanofiber-based phase change materials for thermal management,” *J Colloid Interface Sci*, vol. 629, pp. 478–486, 2023, doi: 10.1016/j.jcis.2022.08.132.

[81] T. Qian, J. Li, X. Min, W. Guan, Y. Deng, and L. Ning, “Enhanced thermal conductivity of PEG/diatomite shape-stabilized phase change materials with Ag nanoparticles for thermal energy storage,” *J Mater Chem A Mater*, vol. 3, no. 16, pp. 8526–8536, 2015, doi: 10.1039/C5TA00309A.

[82] T. Wan *et al.*, “Hectorite effects on swelling and gel properties of hectorite/poly(AM/IA) nanocomposite hydrogels,” *Polymer Bulletin*, vol. 72, no. 5, pp. 1113–1125, 2015, doi: 10.1007/S00289-015-1327-2/FIGURES/7.

[83] B. Zalba, J. M. Marín, L. F. Cabeza, and H. Mehling, “Review on thermal energy storage with phase change: Materials, heat transfer analysis and applications,” *Appl Therm Eng*, vol. 23, no. 3, pp. 251–283, 2003, doi: 10.1016/S1359-4311(02)00192-8.

[84] M. Ghalambaz and J. Zhang, “Conjugate solid-liquid phase change heat transfer in heatsink filled with phase change material-metal foam,” *Int J Heat Mass Transf*, vol. 146, 2020, doi: 10.1016/J.IJHEATMASSTRANSFER.2019.118832.

[85] Y. He, H. Li, F. Luo, Y. Jin, B. Huang, and Q. Qian, “Bio-based flexible phase change composite film with high thermal conductivity for thermal energy storage,” *Compos Part A Appl Sci Manuf*, vol. 151, 2021, doi: 10.1016/j.compositesa.2021.106638.

[86] Y. KONUKLU, F. ERZİN, H. B. AKAR, and A. M. TURAN, “Cellulose-based myristic acid composites for thermal energy storage applications,” *Solar Energy Materials and Solar Cells*, vol. 193, pp. 85–91, 2019, doi: 10.1016/j.solmat.2019.01.006.

[87] J. Zhang, C. H. Zhou, S. Petit, and H. Zhang, “Hectorite: Synthesis, modification, assembly and applications,” *Appl Clay Sci*, vol. 177, pp. 114–138, 2019, doi: 10.1016/J.CLAY.2019.05.001.

[88] W. Xie *et al.*, “A new intumescent insulation emergency material for thermal protection of storage tanks –potassium polyacrylate & organic modified hectorite & intumescent flame retardant,” *J Loss Prev Process Ind*, vol. 76, 2022, doi: 10.1016/j.jlp.2022.104735.

[89] J. A. Diaz *et al.*, “Thermal conductivity in nanostructured films: From single cellulose nanocrystals to bulk films,” *Biomacromolecules*, vol. 15, no. 11, pp. 4096–4101, 2014, doi: 10.1021/BM501131A.

[90] F. Xue, Y. Lu, X. dong Qi, J. hui Yang, and Y. Wang, “Melamine foam-templated graphene nanoplatelet framework toward phase change materials with multiple energy conversion abilities,” *Chemical Engineering Journal*, vol. 365, pp. 20–29, 2019, doi: 10.1016/j.cej.2019.02.023.

[91] Z. Shen, S. Kwon, H. L. Lee, M. Toivakka, and K. Oh, “Enhanced thermal energy storage performance of salt hydrate phase change material: Effect of cellulose nanofibril and graphene nanoplatelet,” *Solar Energy Materials and Solar Cells*, vol. 225, 2021, doi: 10.1016/j.solmat.2021.111028.

[92] Q. F. Guan *et al.*, “Lightweight, tough, and sustainable cellulose nanofiber-derived bulk structural materials with low thermal expansion coefficient,” *Sci Adv*, vol. 6, no. 18, 2020, doi: 10.1126/SCIADV.AAZ1114.

[93] Y. Wang *et al.*, “Facile Fabrication of Robust and Stretchable Cellulose Nanofibers/Polyurethane Hybrid Aerogels,” *ACS Sustain Chem Eng*, vol. 8, no. 24, pp. 8977–8985, 2020, doi: 10.1021/acssuschemeng.0c01564.

[94] Q. Zhang, B. Chen, K. Wu, B. Nan, M. Lu, and M. Lu, “PEG-filled kapok fiber/sodium alginate aerogel loaded phase change composite material with high thermal conductivity and excellent shape stability,” *Compos Part A Appl Sci Manuf*, vol. 143, 2021, doi: 10.1016/j.compositesa.2021.106279.

[95] T. Qian, J. Li, X. Min, W. Guan, Y. Deng, and L. Ning, “Enhanced thermal conductivity of PEG/diatomite shape-stabilized phase change materials with Ag nanoparticles for thermal energy storage,” *J Mater Chem A Mater*, vol. 3, no. 16, pp. 8526–8536, 2015, doi: 10.1039/C5TA00309A.

[96] Y. Qian *et al.*, “Enhanced Thermal-to-Flexible Phase Change Materials Based on Cellulose/Modified Graphene Composites for Thermal Management of Solar Energy,” *ACS Appl Mater Interfaces*, vol. 11, no. 49, pp. 45832–45843, 2019, doi: 10.1021/ACSAMI.9B18543.

[97] V. Pakharenko *et al.*, “Cellulose nanofiber thin-films as transparent and durable flexible substrates for electronic devices,” *Mater Des*, vol. 197, 2021, doi: 10.1016/j.matdes.2020.109274.

[98] A. R. Akhiani, H. S. Cornelis Metselaar, B. C. Ang, M. Mehrali, and M. Mehrali, “Highly hydrophobic silanized melamine foam for facile and uniform assembly of graphene nanoplatelet towards efficient light-to-thermal energy storage,” *Mater Today Energy*, vol. 28, 2022, doi: 10.1016/j.mtener.2022.101077.

[99] H. Bin Yang *et al.*, “Edible, Ultrastrong, and Microplastic-Free Bacterial Cellulose-Based Straws by Biosynthesis,” *Adv Funct Mater*, vol. 32, no. 15, 2022, doi: 10.1002/ADFM.202111713.

[100] L. Tang *et al.*, “Bacterial cellulose/MXene hybrid aerogels for photodriven shape-stabilized composite phase change materials,” *Solar Energy Materials and Solar Cells*, vol. 203, 2019, doi: 10.1016/J.SOLMAT.2019.110174.

[101] T. Kondo and C. Sawatari, “Intermolecular hydrogen bonding in cellulose/poly(ethylene oxide) blends: thermodynamic examination using 2,3-di-O- and 6-O-methylcelluloses as cellulose model compounds,” *Polymer (Guildf)*, vol. 35, no. 20, pp. 4423–4428, 1994, doi: 10.1016/0032-3861(94)90102-3.

[102] M. Mehrali *et al.*, “Investigation of thermal conductivity and rheological properties of nanofluids containing graphene nanoplatelets,” *Nanoscale Res Lett*, vol. 9, no. 1, pp. 1–12, Jan. 2014, doi: 10.1186/1556-276X-9-15/FIGURES/12.

[103] C. Chang *et al.*, “Bioinspired roll-to-roll solar-thermal energy harvesting within form-stable flexible composite phase change materials,” *J Mater Chem A Mater*, vol. 8, no. 40, pp. 20970–20978, 2020, doi: 10.1039/D0TA07289C.

[104] F. Xiong *et al.*, “Copper Sulfide Nanodisk-Doped Solid-Solid Phase Change Materials for Full Spectrum Solar-Thermal Energy Harvesting and Storage,” *ACS Appl Mater Interfaces*, vol. 13, no. 1, pp. 1377–1385, 2021, doi: 10.1021/ACSAMI.0C16891.